

# On the Conceptual Design of a Macro Micro Robot Manipulator for Cochlear Microrobot Operations

Submitted to the Graduate School of Natural and Applied Sciences  
in partial fulfillment of the requirements for the degree of

Master of Science

In Mechanical Engineering

by

Alp Emre YAŞAR

ORCID 0000-0001-6531-3647

August, 2021

This is to certify that we have read the thesis **Title of the Thesis in English** submitted by **Alp Emre Yaşar**, and it has been judged to be successful, in scope and in quality, at the defense exam and accepted by our jury as a MASTER'S THESIS.

**APPROVED BY:**

**Advisor:**                      **Assoc. Prof. Dr. Erkin Gezgin**                      .....

İzmir Kâtip Çelebi University

**Committee Members:**

**Assist. Prof. Dr. Fatih Cemal Can**                      .....

İzmir Kâtip Çelebi University

**Assoc. Prof. Dr. Gökhan Kiper**                      .....

İzmir Institute of Technology University

**Date of Defense: August 27, 2021**

# Declaration of Authorship

I, **Alp Emre Yaşar**, declare that this thesis titled **On the Conceptual Design of a Macro Micro Robot Manipulator for Cochlear Microrobot Operations** and the work presented in it are my own. I confirm that:

- This work was done wholly or mainly while in candidature for the Master's degree at this university.
- Where any part of this thesis has previously been submitted for a degree or any other qualification at this university or any other institution, this has been clearly stated.
- Where I have consulted the published work of others, this is always clearly attributed.
- Where I have quoted from the work of others, the source is always given. This thesis is entirely my own work, with the exception of such quotations.
- I have acknowledged all major sources of assistance.
- Where the thesis is based on work done by myself jointly with others, I have made clear exactly what was done by others and what I have contributed myself.

Signature:

---

Date: 27.08.2021

---

# On the Conceptual Design of a Macro Micro Robot Manipulator for Cochlear Microrobot Operations

## Abstract

Utilization of robotics in medical sciences has initiated many treatment opportunities that are otherwise impossible to be applied. Thanks to exponential technological growth through the field, new solutions, such as the integration of microrobots for surgical operations, have been started to be proposed for a variety of medical cases. One of the controversial scenarios amongst them can be given as the idea of generating hair cells located in cochlea by utilizing stem cell applications inside inner ear. Although the idea emphasized a lot in current medical literature, method of stem cell transfer to the narrow cochlear canals in vivo is still an unclear operation. Thus development of any possible methods that will ensure the usage of medical microrobots in small cochlear workspace is a challenging procedure. In light of this, prior to its structural design, current thesis tries to introduce workspace characterization of a macro-micro surgical robot manipulator that will carry an electromagnetic actuator at its end effector in order to generate motion of untethered microrobot located inside the cochlea. Due to the fact that human head will be a natural obstacle for the manipulator during the treatment, anthropomorphic data of adult individuals were utilized along with the scanned model of inner ear for revealing both obstacle dimensioning and cochlear localization. Throughout the

thesis by the help of acquired data and desired motion characteristics constrained workspace of the micro portion of the manipulator was proposed along with a kinematic synthesis procedure to reveal its workspace optimized conceptual structural design. Due to the fact that acquired results were not sufficient for a compact and payload light design, additional motional constraints were utilized. In light of this a new 5 DoF parallel manipulator design that includes dual end effectors to carry electromagnets for tetherless microrobot actuation inside cochlea was proposed. Throughout the thesis considering newly acquired motional constraints, structural synthesis, kinematic and dynamic analysis procedures of the manipulator were introduced. Theoretical calculations were verified via computer simulation. Following 3D modeling, prototype of the manipulator was manufactured and its hardware verification procedures were carried out by using motion capture cameras and surgical navigation registration methodologies.

**Keywords:** Medical Robotics, Microrobotics, Cochlear Localization, Kinematic Synthesis, Lagrange Dynamics

# Koklear Mikrorobot Operasyonları için bir Makro Mikro Robot Manipülatörünün Tasarımı

## ÖZ

Robotik teknolojilerinin tıp bilimlerinde kullanılması, başka türlü uygulanması mümkün olmayan birçok tedavi olanağını sağlamıştır. Bu alanda görülen teknolojik büyüme sayesinde, çeşitli tıbbi tanılar ve cerrahi operasyonlar için mikro robotların entegrasyonu gibi yeni çözümler önerilmeye başlandı. Aralarındaki tartışmalı senaryolardan biri, iç kulak içinde kök hücre uygulamaları ile kokleada bulunan saç hücrelerinin üretilmesi fikri olarak verilebilir. Bu fikir güncel tıp literatüründe çokça vurgulansa da, in vivo olarak dar koklear kanallara kök hücre transferi yöntemi hala belirsiz bir operasyondur. Bu nedenle, küçük olan koklear çalışma alanlarında tıbbi mikro robotların kullanımını sağlayacak olası yöntemlerin geliştirilmesi zorlu bir işlemdir. Buna müteakiben, mevcut tez, yapısal tasarımından önce, koklea içinde bulunan bağlantısız aktive edilen mikro robotun hareketini oluşturmak için uç efektöründe elektromanyetik aktüatör taşıyacak bir makro-mikro cerrahi robot manipülatörünün çalışma alanı karakterizasyonunu tanıtmaya çalışmaktadır. Tedavi sırasında insan kafasının manipülatör için doğal bir engel olacağından, hem engel boyutlandırmasını hem de koklear lokalizasyonunu ortaya çıkarmak için taranan iç kulak modeli ile yetişkin bireylerin antropomorfik verileri kullanılmıştır. Tez boyunca elde edilen veriler ve istenen hareket özellikleri yardımıyla manipülatörün mikro kısmının kısıtlı çalışma alanı ve çalışma alanı optimize edilmiş kavramsal yapısal tasarımı ortaya çıkarmak için kinematik sentez prosedürü önerilmiştir. Elde

edilen sonuçların kompakt ve hafif tasarım için yeterli olmaması nedeniyle, ek hareket kısıtlamaları kullanılmıştır. Bunun ışığında, koklea içinde bağlantısız çalışan mikrorobot aktivasyonu için elektromıknatısları taşımak üzere çift uçlu efektörler içeren yeni bir 5 serbestlik derecesine sahip paralel manipülatör tasarımı önerildi. Tez boyunca yeni elde edilen hareket kısıtları dikkate alınarak manipülatörün yapısal sentezi, kinematik ve dinamik analiz prosedürleri tanıtılmıştır. Teorik hesaplamalar bilgisayar simülasyonu ile doğrulanmıştır. 3 boyutlu modellemenin ardından manipülatörün prototipi üretilmiş ve hareket yakalama kameraları ve cerrahi navigasyon kayıt metodolojileri kullanılarak donanım doğrulama işlemleri gerçekleştirilmiştir.

**Anahtar Kelimeler:** Medikal Robotlar, Mikrorobotlar, Koklea, Kinematik Sentez, Lagrange Dinamik Model

*to my family...*



# Acknowledgment

On my own behalf, I would like to express my endless gratitude to Assoc. Prof. Dr. Erkin Gezgin who thought me how to be an engineer for people's goodwill. I could only be in one place I would rather be as a Master student. In this context, together with our supervisor, the whole team at İzmir Katip Çelebi Medical Laboratory thinks that we add value to society. I would like to thank my dear friends Seda Özbek, Mertcan Koçak, Didem Güzin, Tuğrul Uslu, Efecan Akdal and Mustafa Volkan Yazıcı for their efforts in this thesis and for giving me friends that I do not want to lose for my entire life. Besides the school life, I would like to thank to my family who did not stop believing me and gave all the support they can within this journey.

Additionally I would like to express my sincere gratitude to The Scientific and Technological Research Council of Turkey. This thesis is supported with Project No: 218E055

# Table of Contents

Declaration of Authorship .....	ii
Abstract .....	iii
Öz .....	v
Acknowledgment .....	viii
List of Figures .....	xi
List of Tables.....	xiv
List of Abbreviations.....	xv
List of Symbols .....	xvi
<b>1 Introduction .....</b>	<b>1</b>
1.1 Scope of the Thesis .....	3
<b>2 Specification of Design Constraints .....</b>	<b>6</b>
2.1 Determination of Cochlea Position in Human Head .....	9
<b>3 Early Structure of Proposed Micro Manipulator.....</b>	<b>14</b>
3.1 Calculating the Average Head Area Measures of an Adult Individual .....	15
<b>4 Kinematic Synthesis .....</b>	<b>17</b>
4.1 Electromagnetic Actuator Design .....	23
<b>5 Micro Manipulator Design Revisions .....</b>	<b>25</b>
5.1 Prototype Production of Hybrid Cartesian Platform Manipulator .....	26
5.2 Updating Micro Manipulator Structural Design .....	29
<b>6 Kinematic and Dynamic Analysis .....</b>	<b>31</b>
6.1 Direct Kinematics .....	31
6.2 Inverse Kinematics.....	33

6.3	Dynamic Analysis .....	35
6.3.1	Trajectory Planning and Verification of the Dynamic Analysis Method .....	40
<b>7</b>	<b>Conceptual Design and Prototyping .....</b>	<b>46</b>
7.1	Micromanipulator Prototype Production .....	48
7.2	Supplementary Studies.....	54
<b>8</b>	<b>Hardware Verification .....</b>	<b>55</b>
<b>9</b>	<b>Conclusion.....</b>	<b>63</b>
	<b>References .....</b>	<b>65</b>
	<b>Appendices .....</b>	<b>70</b>
	<b>Appendix B .....</b>	<b>71</b>
	<b>Curriculum Vitae .....</b>	<b>72</b>

# List of Figures

Figure 1.1	Macro-Micro Manipulator Structure.....	4
Figure 2.1	Cubic Volume that Covers the Adult Human Head Measurements.....	8
Figure 2.2	Working Space of the Concentric Electromagnet Couples.....	9
Figure 2.3	3D Model of the Inner Ear.....	10
Figure 2.4	3D Slicer Visualization Interface .....	10
Figure 2.5	3D Model of the Inner Ear.....	11
Figure 2.6	Obtaining Cochlea Location in Head via Triangulation Method .....	12
Figure 2.7	Cochlea Centered Sphere which Covers the Cubic Volume of Human Head .....	13
Figure 3.1	Electromagnetic couple actuated collinearly on sectioned circle borders .....	14
Figure 3.2	Micro Manipulator Structure (a) and Mutual Central Axis Electromagnets (b).....	15
Figure 4.1	Micro Manipulator Structural Parameters.....	17
Figure 4.2	Kinematic Synthesis Design Configurations.....	20
Figure 4.3	Macro Manipulator Load Capacities.....	21
Figure 4.4	Kinematic Representation of Micro Manipulator in Working Plane .....	23
Figure 4.5	First Trial of Electromagnet Design .....	24
Figure 5.1	Untethered Actuator Motion Scenario.....	25
Figure 5.2	Carbon Rails, Glass Ball Bearings, Teflon Linear Bearings and Polymer Fasteners.....	26
Figure 5.3	Prototype of Cartesian Manipulator .....	27
Figure 5.4	Measurement Rulers and Index Points.....	27
Figure 5.5	Measurement with Three Index Points in the Restricted Protractor Areas .....	28
Figure 5.6	Production of non-slippage joint, Soft Silicone Rubber (a), Silicone ring placed between rotational joint body and inner part (b).....	28

Figure 5.7 Parallel Chain Structure to Ensure Target Electromagnet Movement (R: Rotational Joint, P: Sliding Joint) .....	29
Figure 6.1 Parallel Chain Structural and Variable Parameters .....	31
Figure 6.2 Finding the Electromagnet Position .....	32
Figure 6.3 Finding the Electromagnet Orientation .....	33
Figure 6.4 Inverse Kinematic Analysis: Congruent Angles.....	34
Figure 6.5 Expressing $K_3$ and $K_4$ Constants Using Right Triangle .....	35
Figure 6.6 Dynamic Analysis: Parameters.....	37
Figure 6.7 Expression of System Potential Energy.....	39
Figure 6.8 Transferring Simple Micro Manipulator Model to Simulation Environment.....	40
Figure 6.9 Actuator Position Velocity and Acceleration Graphs.....	52
Figure 6.10 a) Theoretical Actuator Torques and Forces ( ${}^G\mathbf{R}_1$ ) (Mathematica), b) Simulation Environment Actuator Torque and Force ( ${}^G\mathbf{R}_1$ ) (Matlab SimMechanics).....	43
Figure 6.11 a) Theoretical Actuator Torques and Forces ( ${}^G\mathbf{R}_2$ ) (Mathematica), b) Simulation Environment Actuator Torque and Force ( ${}^G\mathbf{R}_2$ ) (Matlab SimMechanics).....	44
Figure 7.1 Micro Manipulator Conceptual Design.....	46
Figure 7.2 Micro Manipulator Kinematic Structure .....	46
Figure 7.3 Micro Manipulator Actuators.....	47
Figure 7.4 Micro Manipulator Part Designs (Other Symmetrical Half of System Not Shown) .....	48
Figure 7.5 Initial Prototype Production Trials Zortrax M200.....	49
Figure 7.6 Prototype Production Stages.....	49
Figure 7.7 Prototype Production and Assembly Stages (Actuator and Carbon Limbs Assembly).....	50
Figure 7.8 Micro Manipulator Assembly Steps .....	50
Figure 7.9 Split Micro Manipulator Arms Assembled & Completed.....	51
Figure 7.10 Connecting the Plexi Glass Part to the CNC Table .....	52
Figure 7.11 Production of Micro Manipulator Floor .....	53
Figure 7.12 Completed Micro Manipulator Assembly I.....	53
Figure 7.13 Completed Micro Manipulator Assembly II.....	53

Figure 7.14 Possible Deformations That May Occur on the Micro Manipulator Ground.....	54
Figure 7.15 Support Parts Designed Between Micro Manipulator Base and Aluminum.....	54
Figure 8.1 Parts Designed for Relation of Physical Measurement Space and Virtual Reality Space.....	55
Figure 8.2 Relation of Physical Measurement Space and Virtual Reality Space.....	55
Figure 8.3 Relation of Micro Manipulator Reference with Physical Measurement Space and Virtual Reality Space .....	56
Figure 8.4 Decisive Zone Apparatus Mounted on Micro Manipulator .....	56
Figure 8.5 Taking Measurements on Decisive Zone Apparatus.....	57
Figure 8.6 Identification of Virtual Reality Environment Index Markings.....	58
Figure 8.7 Micro Manipulator Endpoint Passive IR Reflector Connectors .....	58
Figure 8.8 Manipulator Endpoint Traces and Actuator Trajectories Dedicated to Follow.....	59
Figure 8.9 Hardware Installation .....	59
Figure 8.10 Sending Motion Commands to Actuators via Matlab Simulink.....	60
Figure 8.11 Sending Motion Commands to Actuators via Matlab Simulink.....	60
Figure 8.12 Compensated Joint Space Actuator Trajectories .....	61
Figure 8.13 Confirmation Studies (Compensation) .....	62
Figure 8.14 Validation Studies (New Trajectory).....	62

# List of Tables

Table 2.1	Anthropometric Data Sets Used in the Scope of the Thesis .....	7
Table 2.2	Evaluating Scaling Factor of 3D Inner Ear Atlas.....	11
Table 2.3	Procedure of Triangulation and Calculated Values.....	13
Table 4.1	Kinematic Synthesis Design Parameters and Structural Parameter Results .....	23
Table 6.1	Trajectory Planning Boundary Conditions and Polynomial Coefficients... .....	41
Table 6.2	Micro Manipulator Physical Sizes Determined for Verification .....	45
Table 7.1	Technical Specifications of Micro Manipulator Actuators.....	48
Table 7.2	CNC Production Parameters .....	51

# List of Abbreviations

AESOP	Automated endoscopic system for optimal positioning
SPL	Surgical planning laboratory
İKÇÜ	İzmir Kâtip Çelebi University
STL	Standard tessellation language
DoF	Degrees of freedom
TÜBİTAK	The Scientific and Technological Research Council of Turkey
RRR	R-R-R configuration (3 revolute joints)
CAD	Computer aided design
ABS	Acrylonitrile Butadiene Styrene
CNC	Computerized Numerical Control
IR	Infrared
RMS	Root Mean Square
KUKA	Keller und Knappich Augsburg



# List of Symbols

$({}^G \mathbf{P}_1, {}^G \mathbf{P}_2, {}^G \mathbf{P}_3)$	Points at ear canal entrance
$(d1, d2, d3)$	Perpendicular distances from ear canal entrance to cochlear center
$({}^G x_K, {}^G y_K, {}^G z_K)$	Intersection points (possible cochlear center locations)
$s, \varphi$	Ground location
$d$	Cochlea center location from macro manipulator end point
$R, \phi$	Location of the electromagnets rotational joint
$r$	Radius
$a, b$	Link Lengths
$\theta_1, \theta_2$	Electromagnet location and orientation of the arm
$P_i$	Constant parameters
$f_i$	Variable parameters
$\lambda_1, \lambda_2$	Non-linear Parameters
$F$	Transfer Function
mT	miliTesla
$\omega$	Angular velocity [rad/s]
$K_1, K_2, K_3, K_4$	Constant Parameters
$\alpha$	Angle [rad]
${}^G \mathbf{p}_{mi}$	Vector
${}^G_U \mathbf{R}$	Rotational Matrix
${}^U \mathbf{p}_{mi}$	Macro manipulator endpoint position vectors
$(\tau_1, \tau_2)$	Actuator Torque Couple
F	Force [N]

# Chapter 1

## Introduction

Considering current scientific roadmaps that have been proposed to shape world's research strategies, medical robotics can be given as one of the trending topics of the era. In the 21st century robotic technologies grows exponentially. Horizon 2020 and other strategic institutions create priorities, technologies and strategic developments that shape world's research, development and innovation for future. Medical Robotics and its sub field of surgical robotics is dedicated as one of the trend topics. Medical robotics has subtopics of: Rehabilitation, Collaborative, Assistive and Surgical Robotics. In this thesis report, Surgical robotics is to be investigated.

Thanks to rapid technological developments, many surgical procedures are started to be performed by the assistance of robotic systems such as DaVinci, AESOP, ZEUS, PRECEYES, CorPath, Monarch platform, Mako Rio, Versius and etc. [1-6]. One of the most challenging difficulties that face such techniques are precise control of the instrument and supply of an ergonomic system to the surgeon. Compared to other minimally invasive surgery approaches, robot-assisted surgery potentially gives the surgeon allowing the maximum range of motion and precision as well as a better view of the surgical site. Such studies [7] showed the interdisciplinary research topics, which aim for implementing an efficient and reliable assistive micro robotic system, dedicated to surgery. Every movement the surgeon makes is replicated precisely by the robot. Trials are performed in literature [8] on cadavers in order to implement technique for robotic system in surgery. On the other hand, investigations on surgical robotics has a significant potential to be a less traumatic and more accurate minimally invasive surgery [9].

On the other hand, although promising results have been achieved so far, due to the component limitations such as minimum attainable sizes of actuators, joints and links of the robot mechanisms for the required tasks, utilization areas of the robotic surgery are still limited. Thus, a new subfield of robotic surgery has been emerged by means of micro robots to overcome these limitations.

Micro robotics, which is a subtopic of the surgical robotics will bring insight for new technologies. Micro robotics is the field of miniature robotics, in particular mobile robots with characteristic dimensions less than 1 mm. Since working on a micro dimension, invasiveness of the procedure is reduced. Despite from other systems, micro robotics may work in smaller and complex regions in human body. Micro robotics have different applications: Wirelessly controlled, swallowable and injectable microrobots are investigated during the literature review [10]. Edd et al. designated the working environment of the swimming microrobot for a human kidney with the ability to kidney stone destruction [11]. Dahroug et al. focused on the cholesteatoma surgery and presented the robotic systems that may be implemented to the ear surgery [12]. Amokrane et al. designed the macro-micromanipulator to hold drug implemented microrobot by magnetic field through the human ear canal [13]. Additionally, Grady et al. created three-dimensional remote magnetic manipulation to the microrobot [14]. Furthermore, studies are carried out in order to increase dexterity of regular operations Gezgin et al. proposed the new concept for endoscopic application with high degrees of freedom manipulator [15]. To sum up, working areas of micro robotics are widespread. In this thesis, ear (inner ear, cochlea) is the mainly focused topic.

In light of current scientific literature on micro robotics and ongoing advances, this study tries to propose a conceptual design and a case study for cochlear micro robot operations that are targeted to overcome hearing loss. Hearing loss is a frequent debilitation nowadays. Today, around 466 million people worldwide have disabling hearing loss, and 34 million of these are children [16]. Reasons behind them can be categorized as: environmental factors, infection, inadvertent ototoxic treatments and genetic predisposition all contribute to hair cell loss. Most of the non-mammalians [17], humans and other mammals cannot regenerate hair cells. Cochlear implants represent a technological breakthrough [18], but they still cannot fulfill the functional

discriminate sound in a desired frequency. After literature review recent approaches to hair cell regeneration for inner ear regeneration have been investigated. One concern for the use of induced pluripotent stem (iPS) cells in the treatment of human diseases is the length of time required for the development of individual iPS cell lines [19]. It will likely require support from other techniques, such as the damage-free injection [20]. Researchers need to develop a practical method for clinicians to determine this status [21].

0.3 mm spherical body, which will be covered with stem cells to be actuated using untethered approach. Although main reasons for hearing loss differs for various cases, they can be categorized as environmental factors, infections, inadvertent ototoxic treatments and genetic predisposition that contributes to auditory hair cell losses [22]. Considering the fact that hair cell self-regeneration is not possible for mammals [23], cochlear workspace, where hair cells reside, is so small to be reached by classical surgery operations. Hair cell restoration, and hair loss treatment is a big challenge in related scientific areas. While using cochlear implants still exists as a technological breakthrough to get rid of hearing loss [24], they are not able provide desired effectiveness. Thus recent scientific approaches focus on the possibility to regenerate hair cells by utilizing stem cell transplantation. Despite the potential of producing hair cells from stem cells is still unclear today as well as the future success rates of the possible treatments, there exist many prerequisites to be achieved in order to clarify and proceed through the proposed idea including differentiation of stem cells into cochlear hair cells, transferring stem cells to the cochlea for intracochlear transplantation, and most importantly assuring survival of transferred stem cells by utilizing an efficient way of homing stem cells to the desired locations [25-27].

## 1.1 Scope of the Thesis

Today, with the rapidly developing technology, the use of robot manipulators has become widespread in many areas. The most important element in robot manipulator applications, which aim to reduce human effort in any field and increase task efficiency, usually is that the manipulator end-point can be delivered to a desired position in the relevant working space within the specified precision limits. However,

many studies aimed at capturing relevant precision points within the scope of uncertainties such as unmeasurable bends in manipulator structures are addressed in the literature. Although it is a solution-oriented approach to increase the rigidity and weight of the manipulator to avoid uncertainties in applications where precision is very important, similar solutions also bring negative elements such as the decreasing of the manipulator end-point speed, the precision problems of the manipulator structure and the high torque requirement in the actuators [28]. In this direction, a different perspective given to the problem of the macro-micro manipulator concept, which was first proposed in the last quarter of the last century [28].

The macro-micro robot manipulator structure (Figure 1.1) consists of a macro manipulator responsible for the realization of relatively coarse movements and a micro manipulator that is mounted at the macro manipulator endpoint, responsible for the realization of more precise movements.

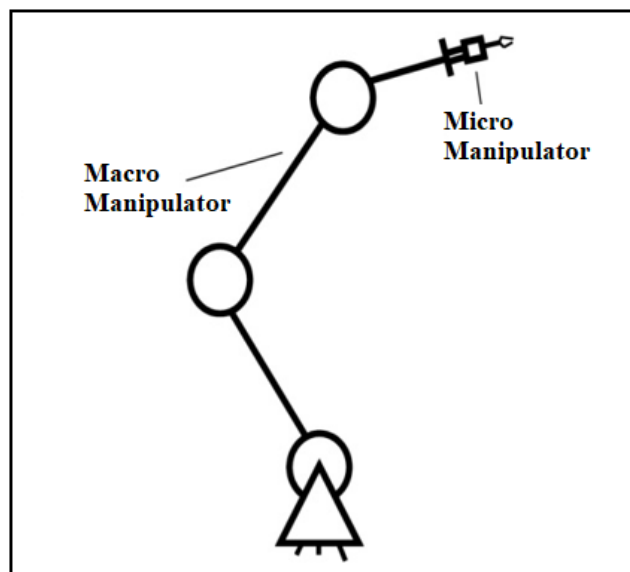


Figure 1.1: Macro-micro manipulator structure

In applications where the macro-micro manipulator structure is used, it is aimed that the micro manipulator carried to the task working space by the macro manipulator can work more precisely locally. In this way, both the accurate working capability provided by the micro manipulator structure and the speed and wide working volume features offered by the macro manipulator structure in local operations are obtained at the same time. Meeting the endpoint precision with two different structures in the relevant manipulator systems enables the micro manipulator to easily compensate the

deviations that may occur in the macro manipulator. Considering the aforementioned superiority, within the scope of the thesis, it was decided to design a robotic surgery system with an electromagnetic actuator that will be designed for stem cell applications in the inner ear area, and which will allow a micro robot placed in the inner ear cochlea to move in a non-contact manner within the cochlear canals, in the structure of a macro-micro robot manipulator.

Surgical manipulator system consists of a six-degree-of-freedom industrial-type serial macro manipulator (KUKA6 R900 SIXX 6) that will be responsible for general movements in the large working space, the micro manipulator mounted on the endpoint of the macro manipulator will be responsible for the manipulating the electromagnets at the end points. The wireless micro robot that is placed in the cochlea with the guidance of the electromagnetic actuator will be the end point of the macro-microsurgery robot manipulator. In this context, it is aimed to create a micro manipulator structure that will carry electromagnetic actuators in the work package carried out in the first period of the thesis process. Related process listed as follow;

- Obtaining the average head dimensions of an adult individual required to create the micro manipulator working volume
- Determination of the approximate location of the cochlea within the head area of the specified dimensions
- Creating micro manipulator structure within the scope of the movement to be followed in the task space
- Performing micro manipulator kinematic and dynamic analysis
- Prototype manufacturing
- Verification of the hardware


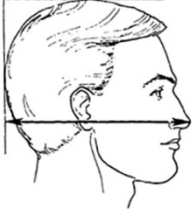

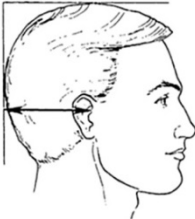
## Chapter 2

# Specification of Design Constraints



Developing new structure relies on the construction parameters. Precision points, which lead the end point of the serial manipulator locations are to be evaluated with human head measurements. Precision points of the end points are selected to have wide range of motion around the determined head measurements. On the other hand, determined points will cause the over lengthen links thus, optimization studies are to be conducted between preferred precision points and link lengths of the arms. Also, while considering structural parameters, working space of the robot carries greater importance. End points and all points on the arms must avoid intersecting with specified spherical space which covers the human head virtually. Safety factors are also included in order not to have any possible collusion with head.

Design considerations related with the human head are briefly explained above. Inside the skull, cochlear location determination will also effect the determination of the construction parameters. Since working space of the manipulator can not be collided with the human head, center of sphere is to be positioned into the center of cochlea. Unfortunately, there is not any unique knowledge related with the cochlea coordinates referenced from certain points on human skull. For every human ear entrance canal length varies in found models having a special scaling factor.

Table 2.1: Anthropometric data sets used in the scope of the thesis [29]

Menton - Head Top Plane (mm)			Pronasal - Head Posterior Plane (mm)		
					
	Female	Male		Female	Male
Average	217.6	232.0	Average	209.7	219.2
Standard Deviation	0.85	0.88	Standard Deviation	0.75	0.80
Maximum	245.0	266.0	Maximum	235.0	247.0
Minimum	187.0	206.0	Minimum	178.0	188.0
Tragus - Head Top Plane (mm)			Tragus - Head Posterior Plane (mm)		
					
	Female	Male		Female	Male
Average	123.5	131.0	Average	97.4	98.9
Standard Deviation	0.55	0.57	Standard Deviation	0.55	0.58
Maximum	145.0	151.0	Maximum	117.0	120.0
Minimum	106.0	112.0	Minimum	80.0	80.0



Tragus – Tragus (mm)			Maximum Frontal Length (mm)		
					
	Female	Male		Female	Male
Average	136.4	144.8	Average	111.3	113.3
Standard Deviation	0.52	0.60	Standard Deviation	0.54	0.52
Maximum	157.0	166.0	Maximum	134.0	134.0
Minimum	115.0	107.0	Minimum	92.0	95.0

As described in Table 2.1, since the averages of male measurements embody the average of female measurements, the relevant cuboid volume is created by taking into account the average male data sets (Figure 2.1).

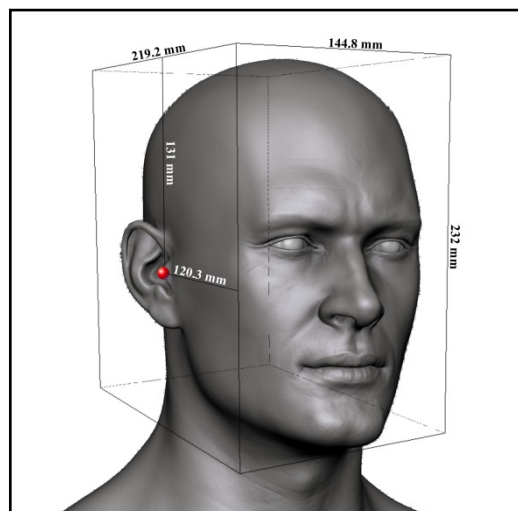


Figure 2.1: Cuboid volume that covers the adult human head measurements

The created volume is an obstacle in the working space according to the pairs of micro manipulators positioned by the macro manipulator in a specific pose. When

the working principle of the coaxial moving electromagnet pairs is examined [30], in order for the micro robot in the cochlea to maintain its position, both electromagnets must be equidistant on the same axis. At this point, working space boundary of the electromagnets in the relevant installation is a cochlea-centered sphere with radius  $r$  that will contain the created cuboid volume constraint (Figure 2.2).

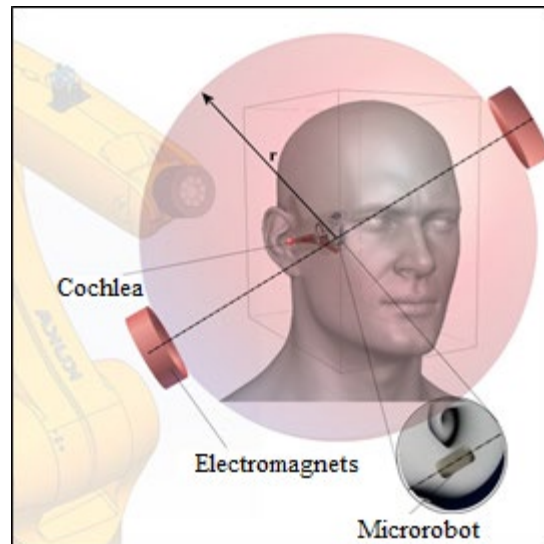


Figure 2.2: Working space of the concentric electromagnet couples

In this way, the closest position where the electromagnet pairs can approach the head area within the given constraint will be on the relevant sphere surface. At this point, in order to determine the radius “ $r$ ”, the approximate coordinates of the cochlea position within the head region must be found.

## 2.1 Determination of Cochlea Position in Human Head

Unfortunately, there is no clear data in the literature regarding the location of the inner ear cochlea region, which was determined with reference to the external ear canal entrance. Although anatomical differences indicate uncertainties regarding the precise location of the cochlea within the skull, an approximate value must be obtained in order to establish the design criteria specified in the previous section. Accordingly, open source study of the SPL inner ear atlas [31-32] presented by Harvard University is used within the scope of the thesis. In the related atlas, there is a three-dimensional model of the inner ear region created using images obtained by scanning with high-resolution CT imaging technique (Figure 2.3).

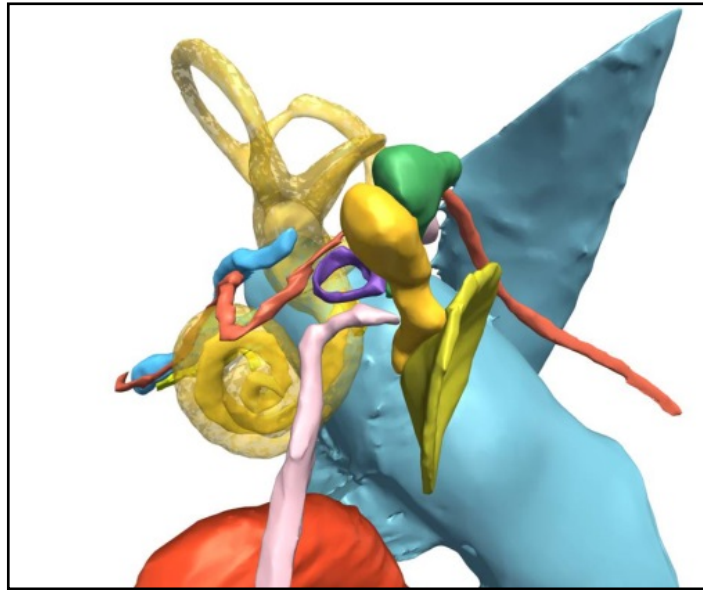


Figure 2.3: 3D model of the inner ear [32]

3D model (Figure 2.3) investigated in software is called 3D Slicer [33-34] which specialize in medical image informatics, image processing, and three-dimensional visualization (Figure 2.4).

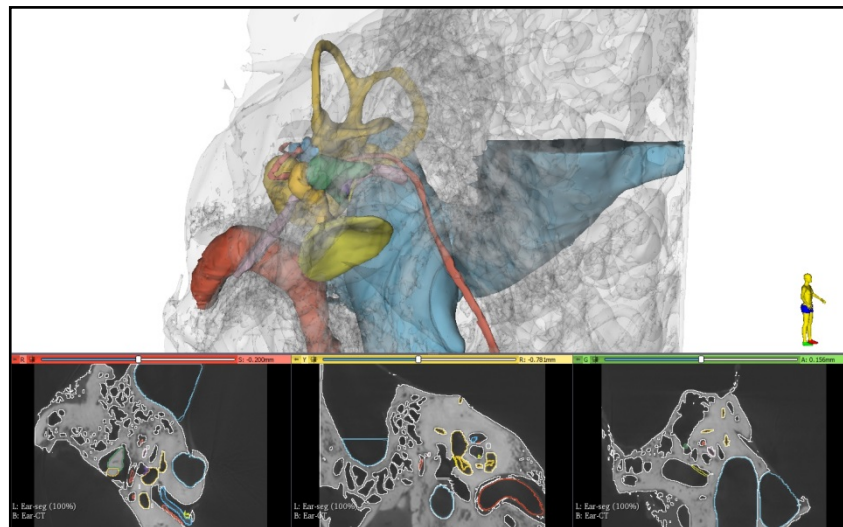


Figure 2.4: 3D slicer visualization interface

3D Slicer program allows to measure the distance from its virtual reference coordinate system to any anatomical point. In order to make precise measurements, unknown scaling effects for 3D models are eliminated in further steps. In this regard, real life malleus, incus and stapes bone measurements will be compared with the Slicer frame measurements.

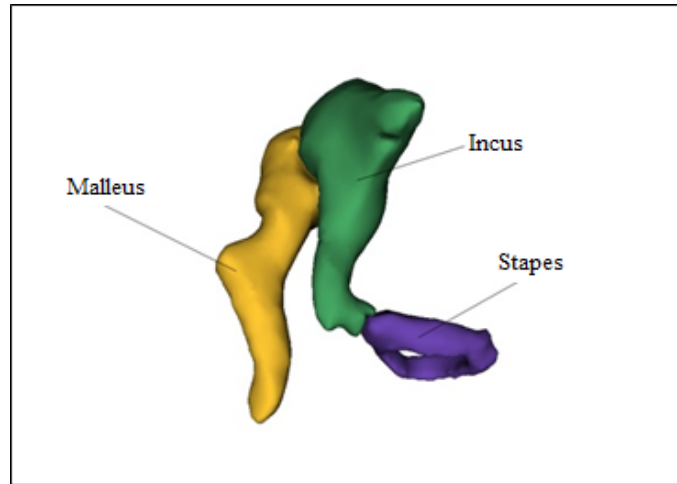


Figure 2.5: 3D model of the inner ear [32]

Salih et al. [35] published high CT scan footages of cat, rat, gerbil and human's three ossicles included with precise measurements. In related research, human ossicles measurements for three different samples are averaged and that value is compared with the 3D Slicer scaled models. In conclusion, ratio between the obtained value and scaled value represents the scaling factor of the atlas (Table 2.2).

Table 2.2: Evaluating scaling factor of 3D inner ear atlas

Salih et al. [35]		SPL Inner Ear Atlas [32]		
Malleus (ML)	4.91 mm	Malleus (Model)	14.80	3.01:1
Incus (IL)	6.32 mm	Incus (Model)	23.11	3.65:1
Stapes (SL)	3.50 mm	Stapes (Model)	11.91	3.40:1
Average Scale				3.35:1

Cochlea location with respect to ear canal entrance point called "G" is to be evaluated. 3 point which are coincident at planar surface of the ear canal entrance

$({}^G\mathbf{P}_1, {}^G\mathbf{P}_2, {}^G\mathbf{P}_3)$  and perpendicular distances ( $d_1, d_2, d_3$ ) to cochlear center are unknown parameters. Parameters to be conducted in equation: Center point of the sphere, perpendicular distances accepted as radius of the spheres ( $d_i$ ).

$$(x - {}^G P_{ix})^2 + (y - {}^G P_{iy})^2 + (z - {}^G P_{iz})^2 = d_i^2 \quad i=1,2,3 \quad (2.1)$$

Three equations (Equation 2.1) are to be used in parameters of triangulation. Roots of the equation will represent different intersection points, thus intersection points that will be covered in cuboid volume for human head are to be accepted as cochlea's center of location  $({}^G x_K, {}^G y_K, {}^G z_K)$ . In this regard, three points are created with respect to cubic volume and reference point. Afterwards, points are transferred into the virtual SPL inner ear atlas model, which are created using the scale obtained in previous section (Figure 2.6).

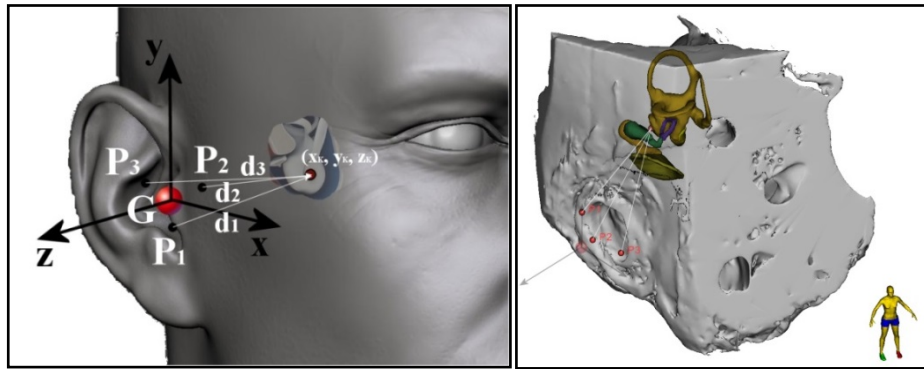


Figure 2.6: Obtaining cochlea location in head via triangulation method

Firstly, distance between 3 points to the cochlear center is obtained in Slicer interface. Three individual distances are converted with scaling factor of the SPL Atlas in order to transfer the model into the real life scale. Result is 3 points with three distances each has direction to cochlea center with respect to real life reference frame. Obtained measurements are the parameters of the Equation 2.1. In order to obtain cochlea center with respect to ear canal entrance, 3-sphere equations and their intersection regions are used (Table 2.3). Important remark to be noted is that interfered planes of the model have minor misalignments with respect to oval shape of the head. STL model X-Y plane parallel to the human skull border plane (temporal bone side) and ear entrance plane has minor distances between them. Since there is no data related with the distance between three planes, required distance is assumed by difference between tragus-tragus to maximum frontal distance (in Table 2.1).

Table 2.3: Procedure of triangulation and calculated values

Real Life Reference System (Cuboid Volume) mm			Virtual Reference System (3D Slicer)		
P <sub>1</sub>	P <sub>2</sub>	P <sub>3</sub>	P <sub>1</sub>	P <sub>2</sub>	P <sub>3</sub>
(10, 0, 0)	(0, 5, 0)	(0, 10, 0)	(135.6, 72.3, -26.7)	(135.6, 38.8, -9.9)	(135.6, 38.8, 6.8)
d <sub>1</sub>	d <sub>2</sub>	d <sub>3</sub>	d <sub>1</sub>	d <sub>2</sub>	d <sub>3</sub>
50.9	45.1	45.4	170.7	151.2	152.2
Cochlear Location			Cochlear Location		
(-21.8, 4.7, -39.5)			(3.27, -34.31, -10.84)		

After the evaluation of coordinates of the cochlea location in human head working space of the manipulator is to be decided. First, cochlea centered spherical volume is to be created which also covers the cuboid volume for human head (Figure 2.1). Radius of the sphere is decided to be 200 mm (Figure 2.7).

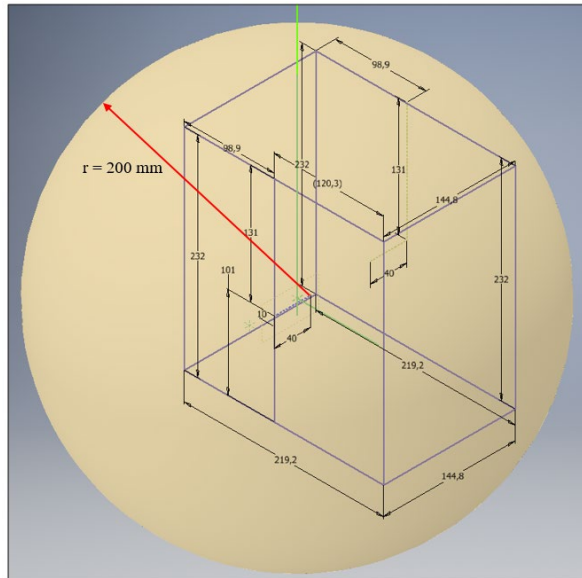


Figure 2.7: Cochlea centered sphere which covers the cubic volume of human head

## Chapter 3

# Early Structure of Proposed Micro Manipulator

Micro manipulator with electromagnet structure comprises two serial arms which works in the same plane and have 3DoF each. Selected structure of micro manipulator is RRR, in order to evaluate coplanar electromagnet couple movements on the cochlea centered sphere (Figure 2.2), micro manipulator link lengths, ground location which is to be located on the macro manipulator and extremum perpendicular distances between macro manipulator to cochlea center are decided.

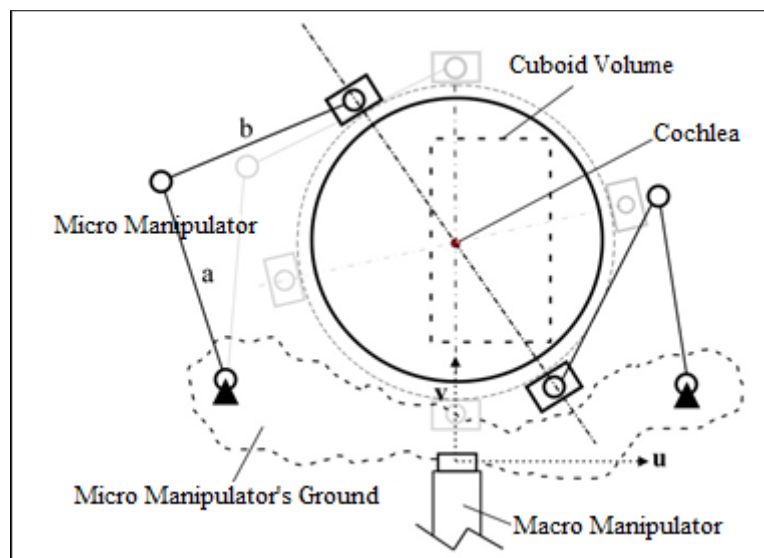
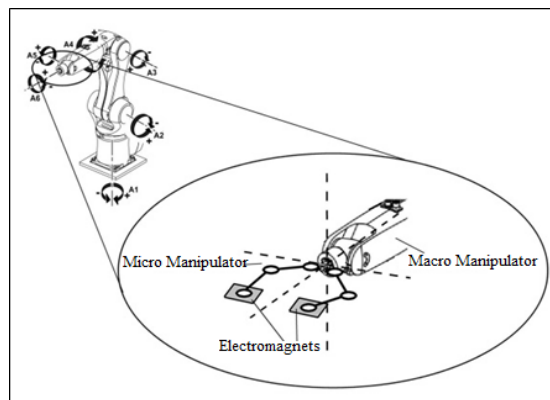


Figure 3.1: Electromagnetic couple actuated collinearly on sectioned circle borders

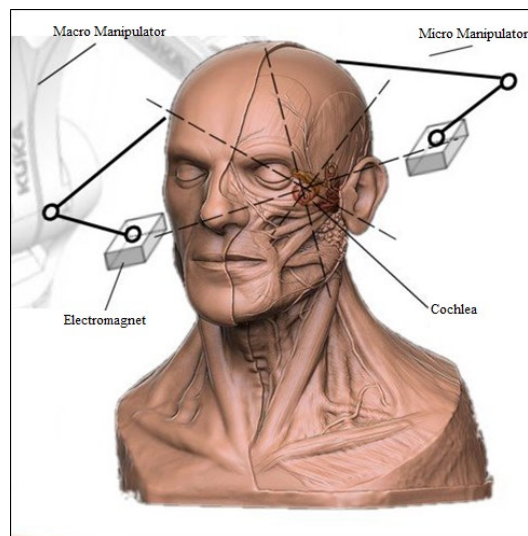
In desired position macro manipulator stands stationary and assembled micro manipulator couple follows the designated path with the restrictions around the sphere represented in Figure 3.1. In this regard, in order to obtain structural parameters kinematic synthesis is performed.

### 3.1 Calculating the Average Head Area Measures of an Adult Individual

As previously stated, the micro manipulator structure, which will carry the electromagnetic actuator at the end, is designed to be composed of two independent planar serial manipulators operating in the same plane and each having three degrees of freedom (Figure 3.2a). The three-dimensional working volume will be achieved by changing the micro manipulator plane by the macro manipulator. It is planned to use the coaxial moving electromagnet pair as the electromagnet installation (Figure 3.2b).



(a)



(b)

Figure 3.2: Proposed Micro Manipulator, Micro Manipulator Structure (a), Mutual Central Axis Electromagnets (b)



In this regard, two electromagnets in the structure of the electromagnetic actuator during the operation can be carried at the ends of different manipulators and posed on the same axis against each other. In order to create an axis on which the micro robot in the cochlea will be located, the link dimensions of the micromanipulator pair must be shaped according to the head area, which is the biggest obstacle in the working volume, and the cochlear position. One of the most important issue here is that the head area measurements for an adult can be determined as one of the design constraints, as the relevant dimensions can vary very easily according to different individual anatomical structures for determination of working space of manipulator, first investigation is about human head measurements from American Soldiers anthropometric data [29].

# Chapter 4

## Kinematic Synthesis

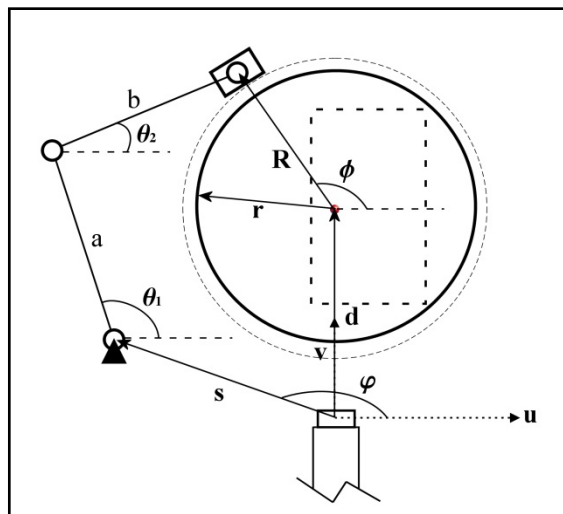


Figure 4.1: Micro manipulator structural parameters

All structural parameters of the micro manipulator couples are shown in Figure 4.1. In figure, “a” and “b” parameters represents link lengths, “s” and “ $\varphi$ ” represents the ground locations with respect to macro manipulator, “d” represents cochlea center location with respect to macro manipulator end point, “R” and “ $\phi$ ” represent location of the electromagnets rotational joint. Electromagnet movements on “R” radius circle are restricted by “r” radius, by means in any orientation of the electromagnets cannot pass through the radius “r”. Restriction results controlling second arm with respect to the first arm movements. Although end effector of a 3 DoF serial manipulator can take any possible poses, the main problem here is the fact that orientation of the second link in order to stay away from the restricted region. Thanks to the fact that the last link can take any orientation that will be tangent to the constraint circle; the main task becomes the body guidance synthesis of 2R serial manipulator. This situation results the micro manipulator to have a restricted degrees of freedom. In this regard, in order for desired orientation to be satisfied, all structural parameters

(a, b, s,  $\phi$ , d, R) are to be designed specially with respect to “r” restriction. Value of “r” which covers the cubic volume of human head is decided in previous sections, accordingly “R” radius is decided with additional safety border section (R=240 mm). Remaining five structural parameters can be evaluated by using kinematic synthesis. In this regard, (Figure 4.1):

$$s + a + b = d + R \quad (4.1)$$

Equation 4.1 includes all variable and constant parameters.  $\theta_2$  and  $\phi$  are directly related with the movement restrictions (electromagnet location and orientation of second arm) which are included in variable parameters ( $\theta_1, \theta_2, \phi$ ). Nevertheless first arm angle ( $\theta_1$ ) do not have such a restriction, thus, related angle is not to be defined in objective function. If  $\theta_1$  is to be left alone while organizing the Equation 4.1,

$$\begin{aligned} a \cos \theta_1 &= R \cos \phi - b \cos \theta_2 - s \cos \phi \\ a \sin \theta_1 &= d + R \sin \phi - b \sin \theta_2 - s \sin \phi \end{aligned} \quad (4.2)$$

Taking squares of the both equation sets and adding them to each other, acquired equation will be without  $\theta_1$  term (Equation 4.3),

$$\begin{aligned} b^2 + R^2 + s^2 + d^2 - a^2 - 2ds \sin \phi + 2bs \sin \phi \sin \theta_2 + 2bs \cos \phi \cos \theta_2 \\ - 2Rs \sin \phi \sin \phi - 2Rs \cos \phi \cos \phi + 2Rd \sin \phi - 2db \sin \theta_2 - 2bR \cos(\phi - \theta_2) = 0 \end{aligned} \quad (4.3)$$

While Equation 4.3 putting in order, constant parameters ( $P_i$ ) and variable parameters ( $f_i$ ) are to be written in polynomial form;

$$\begin{aligned} P_0 f_0 + P_1 f_1 + P_2 f_2 + P_3 f_3 + P_4 f_4 + P_5 f_5 + P_6 f_6 - F &= 0 \\ P_0 &= \frac{b^2 + R^2 + s^2 + d^2 - a^2 - 2ds \sin \phi}{2bR}, f_0 = 1, P_1 = s \sin \phi, f_1 = \frac{\sin \theta_2}{R} \\ P_2 &= s \cos \phi, f_2 = \frac{\cos \theta_2}{R}, P_3 = \frac{d}{b}, f_3 = \sin \phi, P_4 = d, f_4 = -\frac{\sin \theta_2}{R} \\ P_5 &= \frac{s \sin \phi}{b} = \frac{P_1 P_3}{P_4}, f_5 = -\sin \phi, P_6 = \frac{s \cos \phi}{b} = \frac{P_2 P_3}{P_4}, f_6 = -\cos \phi, F = \cos(\phi - \theta_2) \end{aligned} \quad (4.4)$$

Total 5 constant parameter ( $P_i \rightarrow i = 0, 1, \dots, 4$ ) included in Equation 4.4 needs to be evaluated thus, 5 point set ( $\theta_{2j}, \phi_j \rightarrow j = 1, 2, \dots, 5$ ) which fulfills the objective function

will be required. Beforehand, non-linear polynomial acquired from Equation 4.4 is to be transformed into the linear equation. In this regard, non-linear parameters ( $P_5, P_6$ ) are stated as  $\lambda_1$  and  $\lambda_2$

$$P_5 = \lambda_1, P_6 = \lambda_2, P_i = l_i + m_i\lambda_1 + n_i\lambda_2 \rightarrow i = 0, 1, \dots, 4 \quad (4.5)$$

and all remaining constant variables are assumed to be dependent with nonlinear parameters (see Equation 4.5). New polynomial, which comes from Equation 4.4 and 4.5, reorganized, afterwards separating linear and nonlinear parameters,

$$\begin{aligned} l_0f_0 + l_1f_1 + l_2f_2 + l_3f_3 + l_4f_4 &= F \\ m_0f_0 + m_1f_1 + m_2f_2 + m_3f_3 + m_4f_4 &= -f_5 \\ n_0f_0 + n_1f_1 + n_2f_2 + n_3f_3 + n_4f_4 &= -f_6 \end{aligned} \quad (4.6)$$

Three linear polynomials are acquired in Equation 4.6. Five-construction points ( $\theta_{2i}, \phi_i \rightarrow i = 1, 2, \dots, 5$ ) combination with the function design criteria's sets ( $f_i^j, F^j \rightarrow i = 0, 1, \dots, 4 \quad j = 1, 2, \dots, 5$ ) result in total 15 equations with 15 unknowns,

$$\begin{bmatrix} f_0^1 & f_1^1 & f_2^1 & f_3^1 & f_4^1 \\ f_0^2 & f_1^2 & f_2^2 & f_3^2 & f_4^2 \\ f_0^3 & f_1^3 & f_2^3 & f_3^3 & f_4^3 \\ f_0^4 & f_1^4 & f_2^4 & f_3^4 & f_4^4 \\ f_0^5 & f_1^5 & f_2^5 & f_3^5 & f_4^5 \end{bmatrix} \begin{bmatrix} l_0 \\ l_1 \\ l_2 \\ l_3 \\ l_4 \end{bmatrix} = \begin{bmatrix} F^1 \\ F^2 \\ F^3 \\ F^4 \\ F^5 \end{bmatrix}, \mathbf{A} \begin{bmatrix} m_0 \\ m_1 \\ m_2 \\ m_3 \\ m_4 \end{bmatrix} = \begin{bmatrix} -f_5^1 \\ -f_5^1 \\ -f_5^1 \\ -f_5^1 \\ -f_5^1 \end{bmatrix}, \mathbf{A} \begin{bmatrix} n_0 \\ n_1 \\ n_2 \\ n_3 \\ n_4 \end{bmatrix} = \begin{bmatrix} -f_6^1 \\ -f_6^1 \\ -f_6^1 \\ -f_6^1 \\ -f_6^1 \end{bmatrix} \quad (4.7)$$

After that step, unknown parameters can be founded by implementing unknown 15 parameters ( $l_i, m_i, n_i \rightarrow i = 0, 1, \dots, 4$ ) from Equation 4.5 into the Equation 4.7. In order to evaluate 5 constant parameter ( $P_i \rightarrow i = 0, 1, \dots, 4$ ) in objective function and structural parameters (a, b, s,  $\phi$ , d) which also held in objective function, nonlinear parameters ( $\lambda_1, \lambda_2$ ) to be evaluated in Equation 4.8,

$$\begin{aligned} P_5 = \lambda_1 &= \frac{P_1P_3}{P_4} = \frac{(l_1 + m_1\lambda_1 + n_1\lambda_2)(l_3 + m_3\lambda_1 + n_3\lambda_2)}{(l_4 + m_4\lambda_1 + n_4\lambda_2)} \\ P_6 = \lambda_2 &= \frac{P_2P_3}{P_4} = \frac{(l_2 + m_2\lambda_1 + n_2\lambda_2)(l_3 + m_3\lambda_1 + n_3\lambda_2)}{(l_4 + m_4\lambda_1 + n_4\lambda_2)} \end{aligned} \quad (4.8)$$

As a result of the synthesis process, all the structural parameters of a system that can achieve the targeted motion expressed by using five design points will be calculated. Figure 4.2 shows five possible design configurations.

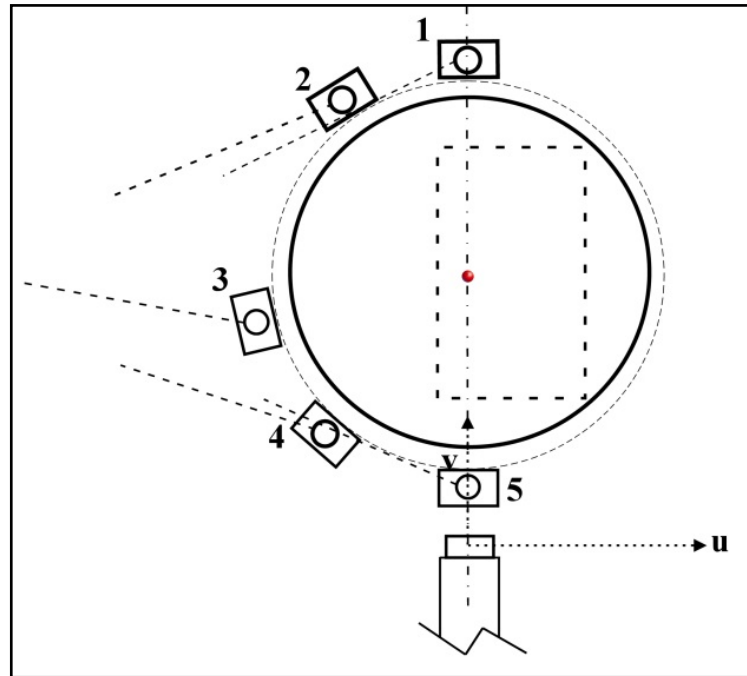


Figure 4.2: Kinematic synthesis design configurations

As can be easily understood from the Figure 4.2, the top and bottom configurations (1 and 5) are the design points that have the greatest effect on the shaping of the structural parameters, as they create the extreme poses for the micro manipulator. For this reason, by changing the design points (2, 3, and 4) in the synthesis process, the short link lengths, the proximity of the fixed link to the macro manipulator end point and the distance that the macro manipulator can approach to the center of the cochlea is greater than the radius "R". However, since the load carrying capacity of the macro manipulator to be used within the scope of the thesis is limited (6 kg) furthermore this capacity decreases as the end axis moves away from the reference point (Figure 4.3). Although there is a freedom by changing the design points, the proposed synthesis method can be compared to the macro manipulator end point. Parameters of  $s$  and  $\phi$  indicating the position of the micro manipulator fixed link were found to be weak while trying to increase improvement.

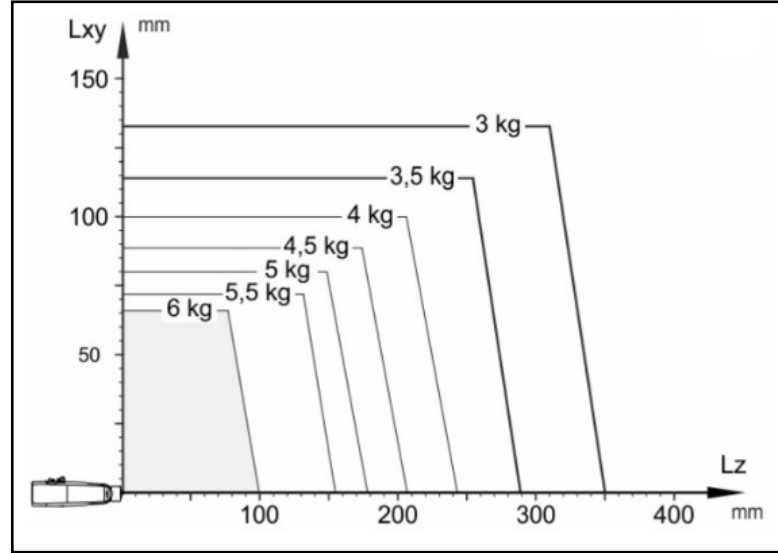


Figure 4.3: Macro manipulator load capacities

In this regard, it was decided to give the relevant parameters ( $s$  and  $\varphi$ ) as design criteria and the task function given in equation 4.4 was updated.

$$P_0 f_0 + P_1 f_1 + P_2 f_2 + P_3 f_3 - F = 0$$

$$P_0 = \frac{b^2 + R^2 + s^2 + d^2 - a^2}{2Rs}, f_0 = 1, P_1 = b, f_1 = \frac{1}{R} \cos(\varphi - \theta_2) - \frac{1}{s} \cos(\varphi - \theta_2) \quad (4.9)$$

$$P_2 = d, f_2 = \frac{1}{s} \sin \varphi - \frac{1}{R} \sin \varphi, P_3 = db = P_1 P_2, f_3 = -\frac{1}{Rs} \sin \theta_2, F = \cos(\varphi - \varphi)$$

In Equation 4.9, there are three constant parameters ( $P_i \rightarrow i = 0, 1, 2$ ) to be calculated, so besides the  $s$  and  $\varphi$  parameters, three design point sets, which consists variable parameters, ( $\theta_{2j}, \phi_j \rightarrow j = 1, 2, 3$ ) will be required to provide the task function.

However, before starting the solution, the nonlinear polynomial obtained in Equation 4.9 should also be linearized. At this point, by expressing with nonlinear parameters ( $P_3$ ) by  $\lambda$ , it is accepted that all remaining constant parameters,

$$P_3 = \lambda, P_i = l_i + m_i \lambda \rightarrow i = 0, 1, 2 \quad (4.10)$$

are dependent on nonlinear parameters as specified in Equation 4.10. If the new polynomial obtained using Equations 4.9 and 4.10 is rearranged and decomposed,

$$l_0 f_0 + l_1 f_1 + l_2 f_2 = F$$

$$m_0 f_0 + m_1 f_1 + m_2 f_2 = -f_3 \quad (4.11)$$

two linear polynomials specified in Equation 4.11 are obtained. When each variable function in Equation 4.11 is evaluated using three sets of design points  $(\theta_{2j}, \phi_j \rightarrow j=1,2,3)$  to be given as design criteria  $(f_i^j, F^j \rightarrow i=0,1,2, j=1,2,3)$ , six equations consisting of six unknowns  $(l_i, m_i \rightarrow i=0,1,2)$  are obtained.

$$\begin{bmatrix} f_0^1 & f_1^1 & f_2^1 \\ f_0^2 & f_1^2 & f_2^2 \\ f_0^3 & f_1^3 & f_2^3 \end{bmatrix} \begin{bmatrix} l_0 \\ l_1 \\ l_2 \end{bmatrix} = \begin{bmatrix} F^1 \\ F^2 \\ F^3 \end{bmatrix}, \begin{bmatrix} f_0^1 & f_1^1 & f_2^1 \\ f_0^2 & f_1^2 & f_2^2 \\ f_0^3 & f_1^3 & f_2^3 \end{bmatrix} \begin{bmatrix} m_0 \\ m_1 \\ m_2 \end{bmatrix} = \begin{bmatrix} -f_3^1 \\ -f_3^2 \\ -f_3^3 \end{bmatrix} \quad (4.12)$$

Likewise, using Equation 4.12, 6 unknown parameters  $(l_i, m_i \rightarrow i=0,1,2)$  in Equation 4.10 can be calculated. In order to calculate three constant parameters  $(P_i \rightarrow i=0,1,2)$  in the task function and then the system structural constants (a, b, d) within these parameters, the nonlinear parameter  $(\lambda)$  must be calculated using Equation 4.13.

$$P_3 = \lambda = P_1 P_2 = (l_1 + m_1 \lambda)(l_2 + m_2 \lambda) \quad (4.13)$$

As a result, all structural parameters of a system that can achieve the target constraints are calculated by using Equations 4.9, 4.12 and 4.13. Increasing design point variations  $(\theta_{2j}, \phi_j, s, \varphi \rightarrow j=1,2,3)$  will also contribute to parameter optimization.

In this regard, in order to calculate the micro manipulator structural parameters to be used within the scope of the thesis, the design points containing the extreme poses of the micro manipulator were determined, and s and  $\varphi$  variables were constantly renewed throughout the optimization procedure so that the position of the micro manipulators fixed link remained within the area specified for the highest load value in Figure 4.3. The results obtained are filtered within the following constraints in order to find the most suitable structural parameters for the study area,

- The ratio between different link lengths does not exceed 1.5 times, taking into account the consistency of the working area and manipulator structure.
- The distance that the macro manipulator can approach perpendicular to the center of the cochlea is greater than the safe sphere radius.

The design points used in the calculation process and the optimized results obtained are given in Table 4.1.

Table 4.1: Kinematic Synthesis Design Parameters and Structural Parameter Results

i	S (mm)	$\Phi^\circ$	R (mm)	$\theta_{2i}^\circ$	$\phi_{2i}^\circ$
1	100	126	240	23	90
2				50	180
3				340	270
a (mm)		b (mm)		d (mm)	
604.8		626.8		398.8	

In addition, the working area of the mechanism and its scaled kinematic representation can be seen in Figure 4.4.

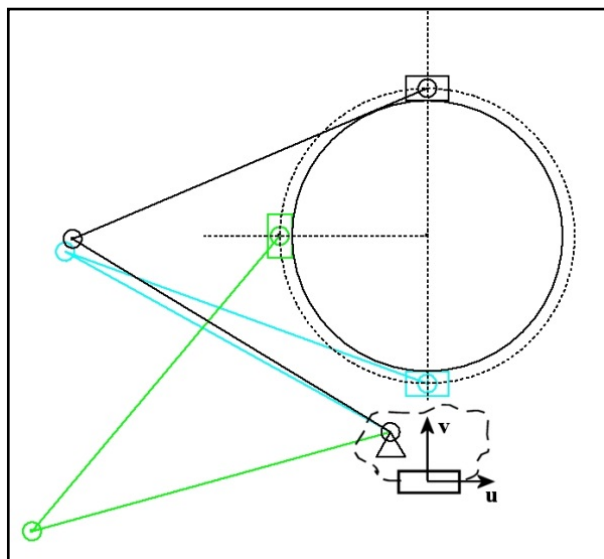


Figure 4.4: Kinematic representation of micro manipulator in working plane

## 4.1 Electromagnetic Actuator Design

Design of the system consists of two electromagnetic couple, which are actuated collinearly (Figure 4.5). In case the electromagnets are in a certain starting position, the projection of the middle of the distance to each other on the determined coaxial axis is determined as the operating point for this actuator structure. If two electromagnets are equidistant from this working point, this state of the structure is



defined as a symmetrical configuration and is used to impose a homogeneous magnetic field on a magnetic particle placed at the working point. If two electromagnets are at different distances to this working point, this state of the structure is defined as an asymmetric configuration and is used to impose a gradient magnetic field on a magnetic particle placed at the working point. The concentric electromagnetic actuator is conceptually suitable for realizing the necessary effects for remote micro particle position control. In the continuation of this study, analyzes were carried out for the sizing of this actuator in accordance with system constraints. Since the parallel study that is related with the manipulator design has been done studies follows the outputs of the parallel study.

In this regard, initially two identical electromagnets are positioned on the same axis, opposite to each other, at a distance of 400 mm between pole surfaces. The reason for this is that the radius of the sphere, which optimally covers the average cuboid volume that will contain the head region of an adult individual created in the previous sections (Figure 2.8), is determined at a radius of 200 mm. Each coil is wrapped in two pieces of steel cores. The cores are composed of two parts, square and rectangular prism.

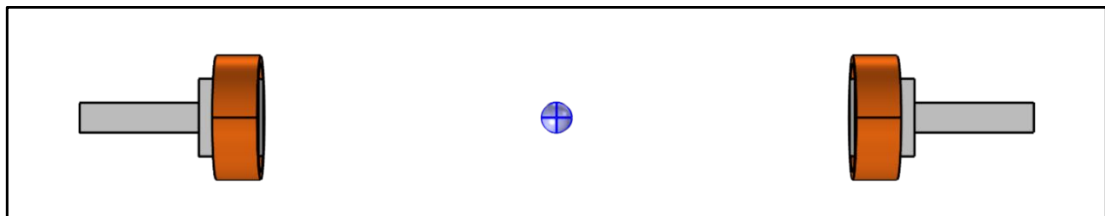


Figure 4.5: First trial of electromagnet design

In order to increase the magnetic field created by the electromagnet pair in the working space, incremental changes were made in other structural parameters in addition to their relative positions. Many trials were made in order to minimize the design of the magnets for space envelope while doing that also the weight of the magnets have been kept low. As a result, with the increase in the length of the core, the length and radius of the coil were redesigned as 45 and 110 mm, respectively. As a second outcome of the analysis performed for this model, a 1.27 mT magnetic field was generated in the center of the cochlea. After the above modification on cores new mass is above 6 kg which is the mass limit that the robotic arm can lift. Due to the fact that the weight of the system could not be carried, a transition was made to the new design.

## Chapter 5

# Micro Manipulator Design Revisions

As can be seen in Table 4.1, the link dimensions calculated by the synthesis method were high. Furthermore, when the studies carried out in electromagnetic actuator design are examined, it is seen that the coaxial moving electromagnet pairs are to be carried at the micro manipulator end point. Used as tethered actuators, without entering the specified sphere containing the cuboid volume, they have high electromagnet weights required to form the desired magnetic field form in the cochlea working volume. Therefore, considering the long links and macro manipulator limited load carrying capacity, it was decided that the RRR open chain micro manipulator pair to be created with the relevant parameters would not be an efficient solution for the macro-micro manipulator system. At this point, in order to reach a solution with a new micro manipulator structure, a new scenario has been created for untethered actuator movement in the light of the studies performed in electromagnetic actuator design (Figure 5.1).

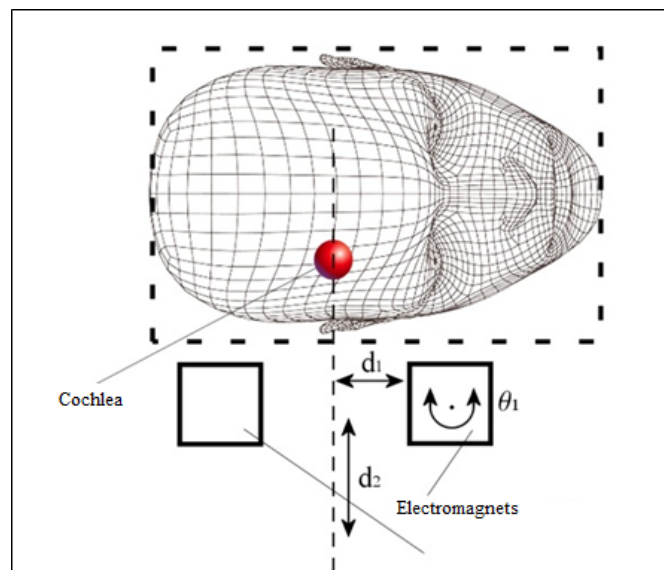


Figure 5.1: Untethered actuator motion scenario

In the new motion scenario shown for a single electromagnet in Figure 5.1, the macro manipulator will bring the untethered actuator to the head region by the cuboid volume where the cochlea is closer. The micromanipulator, whose structural design is to be performed, will be responsible for three independent movements of the electromagnet pairs that will have symmetrical movement: rotation in their own axes ( $\theta_1$ ), translation along the axis between electromagnets ( $d_1$ ) and translation along the macro manipulator end point ( $d_2$ ).

In this regard, before moving on to the updated structural design of the micromanipulator in order to validate the new motion scenario of, a hybrid Cartesian platform manipulator was designed so that electromagnet poses can be obtained in the working volume within the scope of the relevant movements manually to test magnetic field measurements

## 5.1 Prototype Production of Hybrid Cartesian Platform Manipulator

Cartesian manipulator conceptual design was created to include carbon rails, glass ball bearings, teflon linear bearings and polymer connectors (Figure 5.1) in order to prevent the magnetic field form in the target area from being affected during the tests.



Figure 5.2: Carbon rails, glass ball bearings, teflon linear bearings and polymer fasteners

At this point, the three-dimensional design models prepared for production were made of ABS material using the Zortrax M200 rapid prototyping system and all necessary assembly processes were completed (Figure 5.3). The base of the system is made of aluminum sigma profiles in order not to affect the magnetic field form to be tested in the same way.

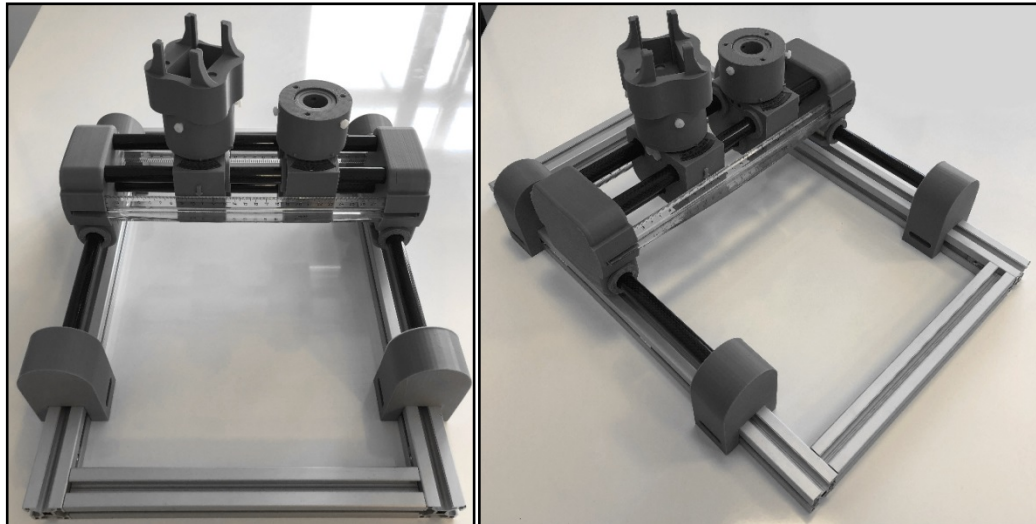


Figure 5.3: Prototype of Cartesian manipulator

Rulers and index points are placed on the system in order to measure the amount of angular orientation and linear movement. Due to the limited location of the protractor, a three-index point design was used, and the  $60^\circ$  scale area could measure a  $180^\circ$  movement (Figures 5.4-5.5).

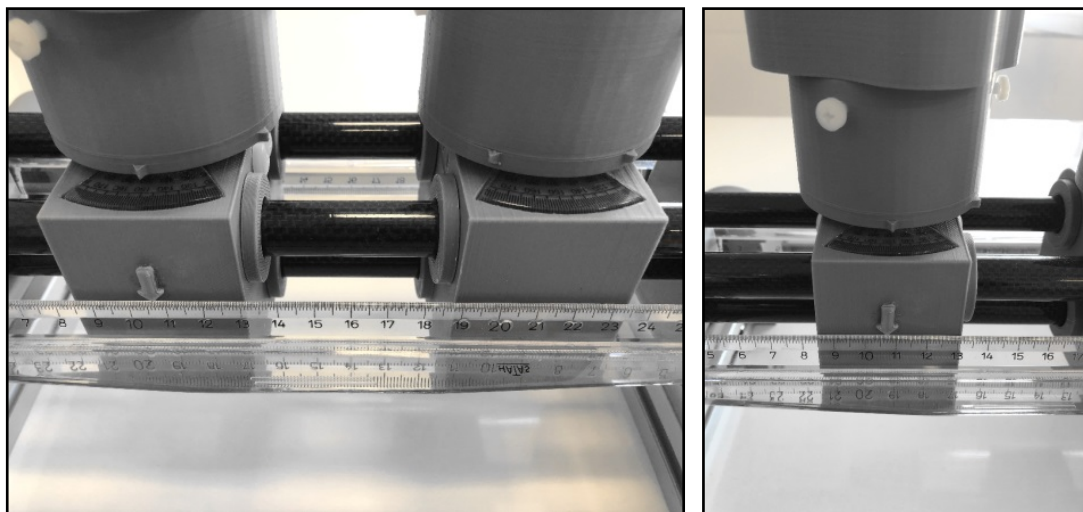


Figure 5.4: Measurement rulers and index points

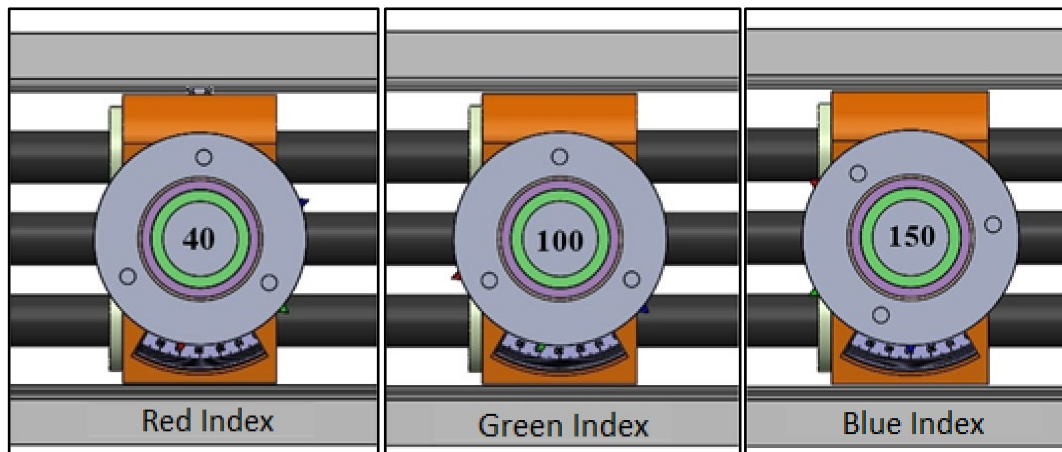


Figure 5.5: Measurement with three index points in the restricted protractor areas

Three polymer bolts are placed on the rotational joint body in order to fix the orientation of the connection apparatus where the magnets will be placed, at the preferred angle. A silicone-based ring is placed between the rotational joint body and the inner part in order to prevent possible slippage by increasing the friction force that will occur between the inner part of the rotational joint and the bolt end point by tightening the polymer bolts (Figure 5.6b).

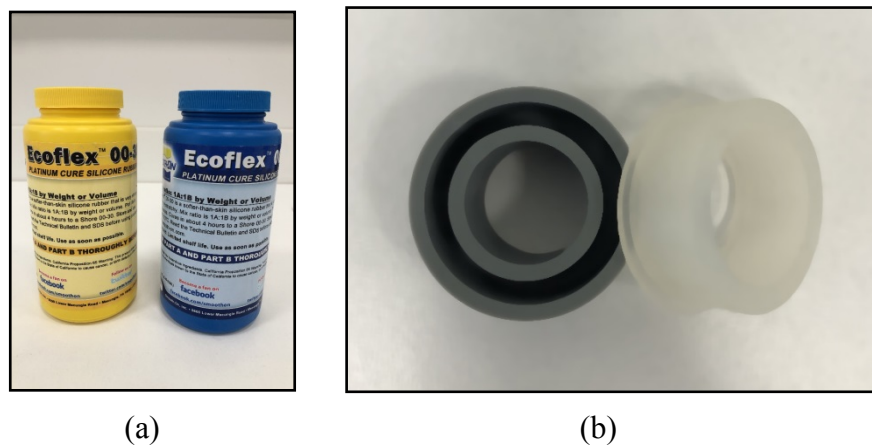


Figure 5.6: Production of non-slippage joint, Soft Silicone Rubber (a), Silicone ring placed between rotational joint body and inner part (b)

In order to produce the relevant part in accordance with the designed system dimensions, a simple mold design was realized, it was produced with a rapid prototyping device and EcoFlex 00-30 mold silicone was poured into it (Figure 5.6a). Silicone rings produced after curing are mounted on the system.

The main purpose at this point is that the simulation studies carried out in the of electromagnetic actuator design will be verified on the designed platform during the

thesis process, and the micromanipulator structural parameters to be redesigned can be updated in the light of the obtained data. Designed Cartesian platform manipulator prototype production is to be done meanwhile in parallel, the structural and parametric design of the micro manipulator to be done, which had to be reconstructed in line with the updated movements.

## 5.2 Updating Micro Manipulator Structural Design

When the new motion scenario designed for the tethered actuator is examined, it is clearly seen that the working volume of the micromanipulator gets closer to the cochlear target (Figure 5.1). This will ensure that the micromanipulator structure to be designed as compact and the endpoint loads (payloads) decrease within the scope of the shorter distances for the magnetic field form that needs to be created. In this context, considering the reduction of the working space to be achieved, it was decided to design a micro manipulator in parallel chain structure instead of series. In this way, firstly precise movement at the micro manipulator end point can be achieved and secondly, the mounting of all manipulator actuators to the fixed link will ensure that the micro manipulator links are lighter under the same endpoint load.

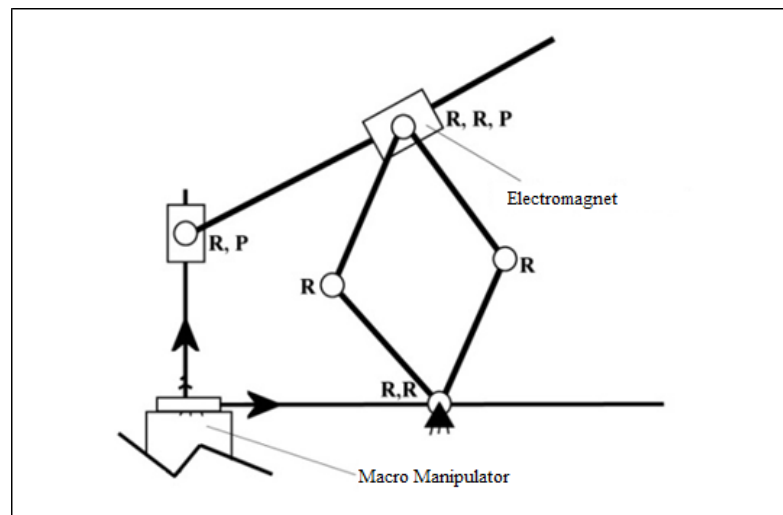


Figure 5.7: Parallel chain structure to ensure target electromagnet movement (**R**: Rotational Joint, **P**: Sliding Joint)

Figure 5.7 shows the kinematic representation of a planar ( $\lambda = 3$ ) parallel chain structure created in the light of the new motion scenario determined for a single electromagnet. When the total degree of freedom ( $M$ ) of the relevant structure is calculated with the Alizade's mobility formulation [35] (Equation 5.1), it is found

that  $M = 3$  and the targeted independent mobility can be achieved with the proposed kinematic structure.

$$M = \sum_{i=1}^j f_i - \sum_{k=1}^L \lambda_k = 9 - 6 = 3 \quad (5.1)$$

In Equation 5.1, " $\sum_{i=1}^j f_i$ " is the total number of degrees of freedom of all joints in the manipulator, "j" the total number of joints, "L" the total number of independent loops, and " $\lambda_k$ " is k it refers to the number of subspaces / spaces in which the closed loop exists. However, system kinematic analysis is required to verify that all target independent motion scenarios can be realized.

# Chapter 6

## Kinematic and Dynamic Analysis

### 6.1 Direct Kinematics

Direct kinematic analysis involves the calculation of the position  $(C_u, C_v)$  and orientation  $(\phi)$  information of the electromagnet at the C point by giving inputs of structural parameters  $(l, d_2)$  and independent actuator variables  $(\theta_1, \theta_2, d_1)$  of the manipulator. As can be seen in Figure 6.1, the link lengths of the five-bar mechanism in kinematic structure are considered equal in order to reduce the system complexity.

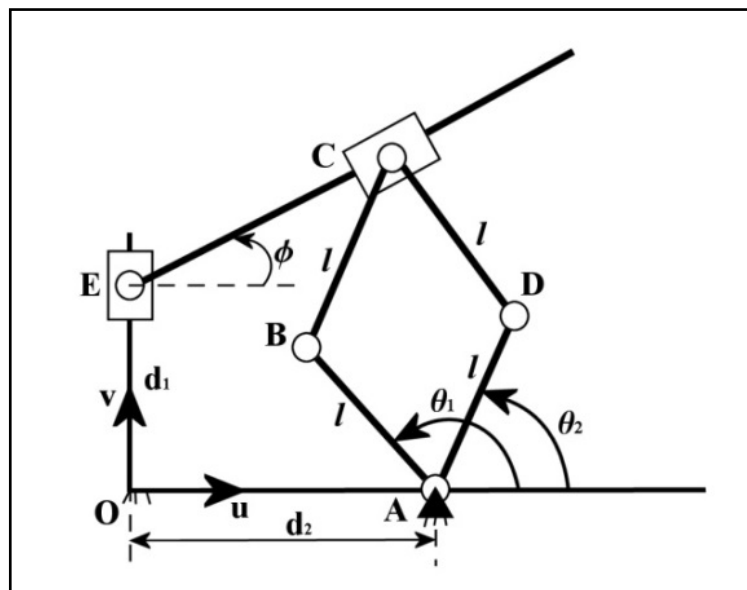


Figure 6.1: Parallel chain structural and variable parameters

Accordingly, the position of the electromagnet  $(C_u, C_v)$  at point C can be easily found using the intersection points of two circles of radius "l" centered B and D. Although two solutions (intersection points) will be obtained, a solution must always be point A  $(d_2, 0)$  because the dimensions of the five-rod links are equal (Figure 6.2).



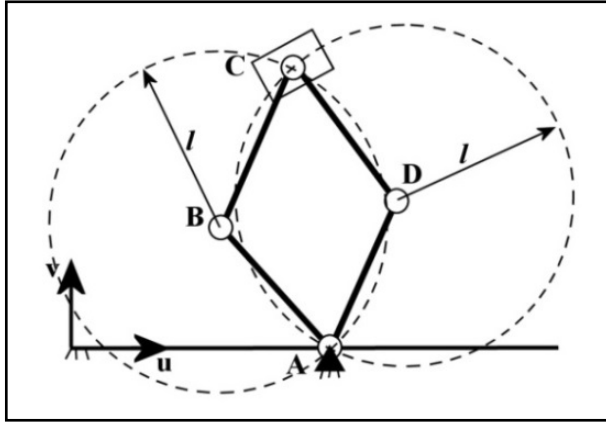


Figure 6.2: Finding the electromagnet position

The positions of points B and D with respect to the reference axes,

$$\begin{aligned} B_u &= d_2 + l \cos \theta_1, & B_v &= l \sin \theta_1 \\ D_u &= d_2 + l \cos \theta_2, & D_v &= l \sin \theta_2 \end{aligned} \quad (6.1)$$

can be calculated using Equation 6.1. The circle equations that accept these points as the center are created in Equation 6.2.

$$\begin{aligned} (u - B_u)^2 + (v - B_v)^2 &= l^2 \\ (u - D_u)^2 + (v - D_v)^2 &= l^2 \end{aligned} \quad (6.2)$$

When both equations are subtracted from each other, when the  $u$  depending on  $v$  (Equation 6.3),

$$u = \frac{d_2 \cos \theta_1 - d_2 \cos \theta_2 - v \sin \theta_1 + v \sin \theta_2}{\cos \theta_1 - \cos \theta_2} \quad (6.3)$$

used in Equation 6.2, the  $v$  parameter ( $C_v$ ) of the electromagnet position at the C point is found.

$$C_v = v = l(\sin \theta_1 + \sin \theta_2) \quad (6.4)$$

Similarly, using Equations 6.3 and 6.4, the  $u$ -parameter of the electromagnet position at the C point is obtained (Equation 6.5).

$$C_u = u = d_2 + l(\cos \theta_1 + \cos \theta_2) \quad (6.5)$$

Electromagnet orientation can be easily calculated using the obtained electromagnet position and its triangle  $\overset{\Delta}{CEF}$  shown in Figure 6.3 (Equation 6.6).

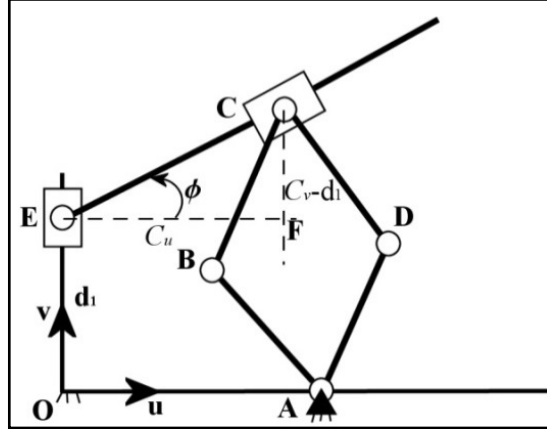


Figure 6.3: Finding the electromagnet orientation

$$\phi = \text{Atan2}(C_v - d_1, C_u) \quad (6.6)$$

Electromagnet velocities and accelerations at point C are obtained by deriving the position and orientation equations (Equation 6.4-6.6) with respect to time (Equation 6.7).

$$\begin{aligned} \frac{dC_v}{dt} &= l(\dot{\theta}_1 \cos \theta_1 + \dot{\theta}_2 \cos \theta_2), & \frac{dC_u}{dt} &= -l(\dot{\theta}_1 \sin \theta_1 + \dot{\theta}_2 \sin \theta_2) \\ \frac{d^2C_v}{dt^2} &= \frac{d}{dt}(l(\dot{\theta}_1 \cos \theta_1 + \dot{\theta}_2 \cos \theta_2)), & \frac{d^2C_u}{dt^2} &= \frac{d}{dt}(-l(\dot{\theta}_1 \sin \theta_1 + \dot{\theta}_2 \sin \theta_2)) \quad (6.7) \\ \ddot{\phi} &= \frac{(d_1 - C_v) \frac{dC_u}{dt} + C_u \left( \frac{dC_v}{dt} - \dot{d}_1 \right)}{C_u^2 + (C_v - d_1)^2}, & \dot{\phi} &= \frac{d\phi}{dt} \end{aligned}$$

## 6.2 Inverse Kinematics

Inverse kinematic analysis includes the calculation of the independent actuator inputs  $(\theta_1, \theta_2, d_1)$  of the manipulator required to reach the relevant position by providing structural parameters  $(l, d_2)$  and the position  $(C_u, C_v)$  and orientation  $(\phi)$  information of the electromagnet at C point.

Accordingly, the relevant actuator inputs can be found easily by using direct kinematic equations (Equation 6.4-6.6).

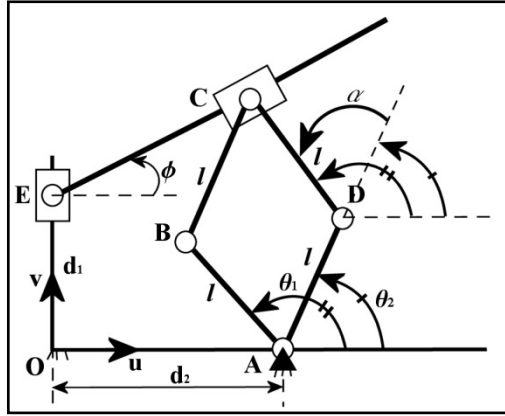


Figure 6.4: Inverse kinematic analysis: Congruent angles

Since the link lengths ( $l$ ) of the kinematic five bar mechanism are equal, the mutual links must always be parallel to each other. At this point, in Equations 6.4 and 6.5 writing  $\alpha + \theta_2$  instead of the input angle  $\theta_1$  (Equation 6.8),

$$\frac{C_v}{l} = \sin(\alpha + \theta_2) + \sin \theta_2$$

$$\frac{C_u - d_2}{l} = \cos(\alpha + \theta_2) + \cos \theta_2$$

(6.8)

when squares are taken and added together, the angle  $\alpha$

$$\alpha = \cos^{-1} \frac{K_1^2 + K_2^2 - 2}{2}, K_1 = \frac{C_v}{l}, K_2 = \frac{C_u - d_2}{l}$$

(6.9)

can be calculated using Equation 6.9. After this step, Equation 6.8 can be rearranged by equating the trigonometric variables contained in it.

$$\begin{aligned} K_1 &= \sin \alpha \cos \theta_2 + \cos \alpha \sin \theta_2 + \sin \theta_2 = K_3 \sin \theta_2 + K_4 \cos \theta_2 \\ K_2 &= \cos \alpha \cos \theta_2 - \sin \alpha \sin \theta_2 + \cos \theta_2 = K_3 \cos \theta_2 - K_4 \sin \theta_2 \\ K_3 &= 1 + \cos \alpha, \quad K_4 = \sin \alpha \end{aligned} \quad (6.10)$$

$K_3$  and  $K_4$  constants in Equation 6.10 can be expressed differently by using Figure 6.5 (Equation 6.11).

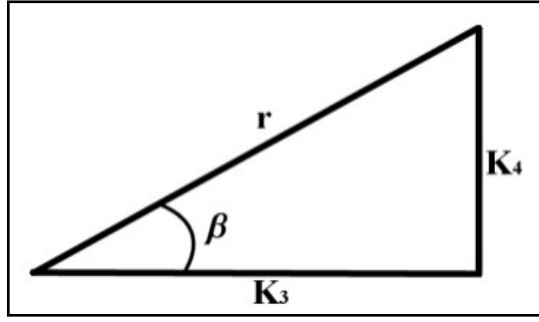


Figure 6.5: Expressing  $K_3$  and  $K_4$  constants using right triangle

$$\begin{aligned} K_3 &= r \cos \beta, \quad K_4 = r \sin \beta \\ r &= \sqrt{K_3^2 + K_4^2}, \quad \beta = \text{Atan2}(K_4, K_3) \end{aligned} \quad (6.11)$$

If Equation 6.10 is rearranged using Equation 6.11,

$$\begin{aligned} \frac{K_1}{r} &= \cos \beta \sin \theta_2 + \sin \beta \cos \theta_2 = \sin(\beta + \theta_2) \\ \frac{K_2}{r} &= \cos \beta \cos \theta_2 - \sin \beta \sin \theta_2 = \cos(\beta + \theta_2) \end{aligned} \quad (6.12)$$

then Equation 6.12 will be obtained. Then using the relevant equations (Equation 6.6-6.12),

$$\begin{aligned} \theta_2 &= \text{Atan2}(K_1, K_2) - \text{Atan2}(K_4, K_3) \\ \theta_1 &= \theta_2 + \cos^{-1} \frac{K_1^2 + K_2^2 - 2}{2} \\ d_1 &= C_v - C_u \tan \phi \end{aligned} \quad (6.13)$$

input angles ( $\theta_1, \theta_2$ ) can be calculated together with the input  $d_1$  (Equation 6.13).

### 6.3 Dynamic Analysis

Although the micro manipulator endpoint speeds during the operation are not high considering the working volume, the dynamic analysis of the proposed mechanism should be performed parametrically in order to select the system actuators according to the load to be carried at the end point. Based on this, the theoretical dynamic analysis of the related system within the scope of the thesis was carried out using the Lagrange formulation.

$$\frac{d}{dt} \left( \frac{\partial L}{\partial \dot{q}_j} \right) - \frac{\partial L}{\partial q_j} = Q_j + \sum_{i=1}^k \lambda_i \frac{\partial \Gamma_i}{\partial q_j}, \quad L = K - U, \quad i \rightarrow 1, \dots, k, \quad j \rightarrow 1, \dots, n \quad (6.14)$$

In Equation 6.14, the first type of Lagrange Equation written according to dependent coordinates is seen. Here,  $q_j$  represents generalized coordinates,  $Q_j$  represents actuator torques and forces,  $\lambda_i$  represents Lagrange factors,  $\Gamma_i$  represents constraint functions,  $K$  and  $U$  are manipulator kinetic and potential energies,  $k$  is the total number of constraint functions and  $n$  is the total number of generalized coordinates. As Tsai stated in [37], Equation 6.14 can be decomposed into  $n$  sets of equations,  $k$  for dependent coordinates and  $n-k$  for actuator variables (Equation 6.15).

$$\begin{aligned} \sum_{i=1}^k \lambda_i \frac{\partial \Gamma_i}{\partial q_j} &= \frac{d}{dt} \left( \frac{\partial L}{\partial \dot{q}_j} \right) - \frac{\partial L}{\partial q_j} - \hat{Q}_j, \quad i \rightarrow 1, \dots, k, \quad j \rightarrow 1, \dots, k \\ Q_j &= \frac{d}{dt} \left( \frac{\partial L}{\partial \dot{q}_j} \right) - \frac{\partial L}{\partial q_j} - \sum_{i=1}^k \lambda_i \frac{\partial \Gamma_i}{\partial q_j}, \quad i \rightarrow 1, \dots, k, \quad j \rightarrow k+1, \dots, n \end{aligned} \quad (6.15)$$

Here  $\hat{Q}_j$  represents the generalized force component of external forces. Friction forces and deformation of the links were neglected within the calculations. In order to compensate the minor differences of the results safety factor is considered for proper torque values. As can be seen in Equation 6.15, the actuator torque and / or forces can be easily calculated by using Lagrange multipliers to be calculated with the help of system kinematics.

In order to derive the constraint equations, three ( $k=3$ ) dependent coordinates,  $C_u, C_v$  and  $\phi$ , are selected on the system.  $\theta_1, \theta_2$  and  $d_1$  are system actuator variables. Thus, six ( $n=6$ ) generalized coordinates were created in the system.

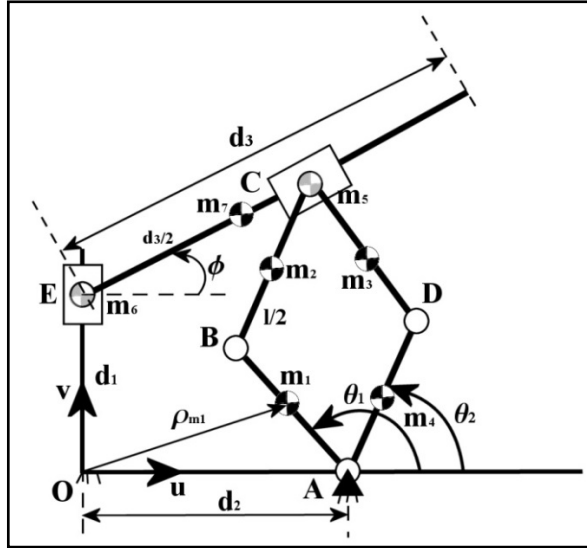


Figure 6.6: Dynamic analysis: Parameters

As can be seen clearly in Figure 6.6, the distance between points B, D, and point C where the electromagnet is located is always constant and equal to  $l$ . Thus, the first and second constraint functions,

$$\begin{aligned}
 \Gamma_1 &= (C_u - B_u)^2 + (C_v - B_v)^2 - l^2 = 0 \\
 \Gamma_1 &= (C_u - d_2 - l \cos \theta_1)^2 + (C_v - l \sin \theta_1)^2 - l^2 = 0 \\
 \Gamma_2 &= (C_u - D_u)^2 + (C_v - D_v)^2 - l^2 = 0 \\
 \Gamma_2 &= (C_u - d_2 - l \cos \theta_2)^2 + (C_v - l \sin \theta_2)^2 - l^2 = 0
 \end{aligned} \tag{6.16}$$

can be written as shown in Equation 6.16. Since the triangle  $\overset{\Delta}{CEF}$  shown in Figure 6.6 will always, occur in the system, the third constraint equation,

$$\begin{aligned}
 \tan \phi &= \frac{C_v - d_1}{C_u} \\
 \Gamma_3 &= C_u \tan \phi - C_v + d_1 = 0
 \end{aligned} \tag{6.17}$$

created as seen in Equation 6.17. Before using Equation 6.15, the kinetic and potential energies of the manipulator, links should be expressed. Due to the system structure, the angular velocities of each link can be written (Equation 6.18).

$$\omega_1 = \omega_3 = \overset{\square}{\theta}_1, \quad \omega_2 = \omega_4 = \overset{\square}{\theta}_2, \quad \omega_5 = \omega_7 = \overset{\square}{\phi}, \quad \omega_6 = 0 \tag{6.18}$$

The linear velocities of the link centroids shown in Figure 6.8 are calculated by taking the derivatives of each center of gravity positions with respect to time (Equation 6.19).

$$\begin{aligned}
\rho_{m1u} &= d_2 + \frac{l}{2} \cos \theta_1, & \frac{d\rho_{m1u}}{dt} &= -\frac{l}{2} \dot{\theta}_1 \sin \theta_1 \\
\rho_{m1v} &= \frac{l}{2} \sin \theta_1, & \frac{d\rho_{m1v}}{dt} &= \frac{l}{2} \dot{\theta}_1 \cos \theta_1 \\
\rho_{m2u} &= d_2 + l \cos \theta_1 + \frac{l}{2} \cos \theta_2, & \frac{d\rho_{m2u}}{dt} &= -l\dot{\theta}_1 \sin \theta_1 - \frac{l}{2} \dot{\theta}_2 \sin \theta_2 \\
\rho_{m2v} &= l \sin \theta_1 + \frac{l}{2} \sin \theta_2, & \frac{d\rho_{m2v}}{dt} &= l\dot{\theta}_1 \cos \theta_1 + \frac{l}{2} \dot{\theta}_2 \cos \theta_2 \\
\rho_{m3u} &= d_2 + l \cos \theta_2 + \frac{l}{2} \cos \theta_1, & \frac{d\rho_{m3u}}{dt} &= -l\dot{\theta}_2 \sin \theta_2 - \frac{l}{2} \dot{\theta}_1 \sin \theta_1 \\
\rho_{m3v} &= l \sin \theta_2 + \frac{l}{2} \sin \theta_1, & \frac{d\rho_{m3v}}{dt} &= l\dot{\theta}_2 \cos \theta_2 + \frac{l}{2} \dot{\theta}_1 \cos \theta_1 \\
\rho_{m4u} &= d_2 + \frac{l}{2} \cos \theta_2, & \frac{d\rho_{m4u}}{dt} &= -\frac{l}{2} \dot{\theta}_2 \sin \theta_2 \\
\rho_{m4v} &= \frac{l}{2} \sin \theta_2, & \frac{d\rho_{m4v}}{dt} &= \frac{l}{2} \dot{\theta}_2 \cos \theta_2 \\
\rho_{m5u} &= C_u, & \frac{d\rho_{m5u}}{dt} &= \frac{dC_u}{dt} \\
\rho_{m5v} &= C_v, & \frac{d\rho_{m5v}}{dt} &= \frac{dC_v}{dt} \\
\rho_{m6u} &= 0, & \frac{d\rho_{m6u}}{dt} &= 0, & \rho_{m6v} &= d_1, & \frac{d\rho_{m6v}}{dt} &= \dot{d}_1 \\
\rho_{m7u} &= \frac{d_3}{2} \cos \phi, & \frac{d\rho_{m7u}}{dt} &= -\frac{d_3}{2} \dot{\phi} \sin \phi \\
\rho_{m7v} &= d_1 + \frac{d_3}{2} \sin \phi, & \frac{d\rho_{m7v}}{dt} &= \dot{d}_1 + \frac{d_3}{2} \dot{\phi} \cos \phi
\end{aligned} \tag{6.19}$$

Total manipulator kinetic energy ( $K$ ) using Equation 6.18 and Equation 6.19,

$$\begin{aligned}
K &= K_1 + K_2 + K_3 + K_4 + K_5 + K_6 + K_7 \\
K_i &= \frac{1}{2} I_{wvi} \omega_i^2 + \frac{1}{2} m_i \left( \left( \frac{d\rho_{miu}}{dt} \right)^2 + \left( \frac{d\rho_{miv}}{dt} \right)^2 \right) \quad i \rightarrow 1, 2, \dots, 7
\end{aligned} \tag{6.20}$$

expressed as seen in Equation 6.20.

Due to the macro-micro manipulator structure, it is necessary to know the orientation  ${}^G \mathbf{R}$  of the micro manipulator end point relative to the macro manipulator global reference (G) and the height (z) of the macro manipulator wrist point in the direction

of gravity in order to express the total micro manipulator potential energy (Figure 6.7).

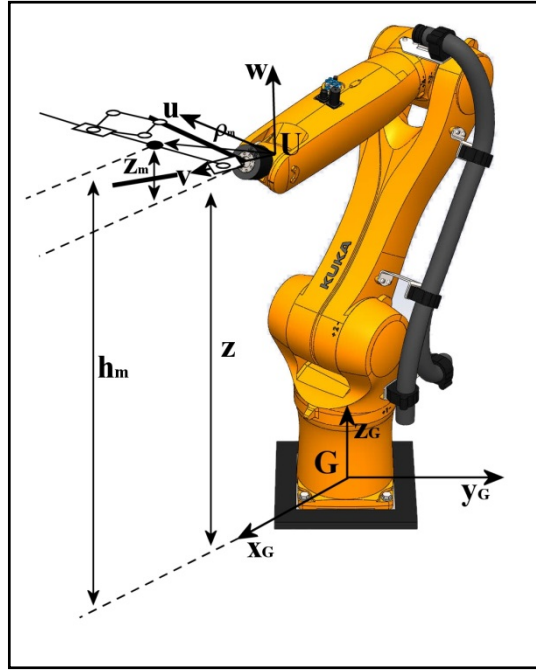


Figure 6.7: Expression of system potential energy

The height of the link centers of gravity according to the global reference system ( $h_{mi}$ ) is obtained by adding the height ( $z$ ) of the macro manipulator wrist point in the direction of gravity and the gravitational components ( $z_m$ ) of the macro manipulator end point position vectors (Equation 6.19) expressed according to the global reference (Equation 6.21).

$$h_{mi} = z_{mi} + z \quad (6.21)$$

The relevant components are calculated using the rotation matrix  ${}^G_U \mathbf{R}$ , which determines the orientation of the macro manipulator endpoint, and the  ${}^G \boldsymbol{\rho}_{mi}$  vector obtained from the product of the center of gravity macro manipulator endpoint position vectors  ${}^U \boldsymbol{\rho}_{mi}$  (Equation 6.21).

$${}^G \boldsymbol{\rho}_{mi} = {}^G_U \mathbf{R} {}^U \boldsymbol{\rho}_{mi}$$

$${}^G_U \mathbf{R} = \begin{bmatrix} r_{11} & r_{12} & r_{13} \\ r_{21} & r_{22} & r_{23} \\ r_{31} & r_{32} & r_{33} \end{bmatrix}, \quad {}^U \boldsymbol{\rho}_{mi} = \begin{bmatrix} {}^U \rho_{miu} \\ {}^U \rho_{miv} \\ 0 \end{bmatrix}, \quad {}^G \boldsymbol{\rho}_{mi} = \begin{bmatrix} x_m \\ y_m \\ z_m \end{bmatrix} \quad (6.22)$$

$$z_m = r_{31} {}^U \rho_{miu} + r_{32} {}^U \rho_{miv}$$



The micro manipulator, which is a planar mechanism, operates in the macro manipulator endpoint  $uv$  plane and the link centroids do not have  $w$  parameters in the local reference. In Equation 6.22, the direction of gravity is considered parallel with the z-axis of the global reference system. At this point, the total micromanipulator potential energy is,

$$U = U_1 + U_2 + U_3 + U_4 + U_5 + U_6 + U_7 \quad (6.23)$$

$$U_i = m_i g h_{mi} \quad i \rightarrow 1, 2, \dots, 7$$

expressed as seen in Equation 6.23. When all relevant equations (Equation 6.16-6.23) are used in Equation 6.15, the actuator torque ( $\tau_1, \tau_2$ ) and force (F), values required for one side of the micro manipulator are calculated.

### 6.3.1 Trajectory Planning and Verification of Dynamic Analysis Method

The theoretical dynamic analysis method presented in previous section must verified in order to use within the thesis. For this reason, a simplified and dimensioned model of the micromanipulator was transferred from the CAD environment to the Matlab SimMechanics simulation environment with mates (Figure 6.8).



Figure 6.8: Transferring simple micro manipulator model to simulation environment

In order to get the actuator torque and force values over the system, simple trajectories are defined for micro manipulator actuators in the joint space. Each trajectory is formed from cubic polynomials (Equation 6.24),

$$\begin{aligned} \theta_1(t) &= A_1 t^3 + B_1 t^2 + C_1 t + D_1 \\ \theta_2(t) &= A_2 t^3 + B_2 t^2 + C_2 t + D_2 \\ d_1(t) &= A_3 t^3 + B_3 t^2 + C_3 t + D_3 \end{aligned} \quad (6.24)$$

The coefficients of the relevant polynomials are calculated from the common solutions of the equation sets created by using the starting and ending boundary conditions specified in Table 6.1 together with Equation 6.24.

Table 6.1: Trajectory planning boundary conditions and polynomial coefficients

<b>Joint Position (radian, m, s)</b>	<b>Joint Velocity</b>
$\theta_1(t=0) = 2.618, \theta_1(t=5) = 2.094$ $\theta_2(t=0) = 0.523, \theta_2(t=5) = 1.047$ $d_1(t=0) = 0.015, d_1(t=5) = 0.025$	$\dot{\theta}_1(t=0) = 0, \dot{\theta}_1(t=5) = 0, \dot{\theta}_2(t=0) = 0$ $\dot{\theta}_2(t=5) = 0, \dot{d}_1(t=0) = 0, \dot{d}_1(t=5) = 0$
<b>Polynomial Coefficients</b>	
$A_1 = 0.00837, B_1 = -0.06283, C_1 = 0, D_1 = 2.61799$ $A_2 = -0.00837, B_2 = 0.06283, C_2 = 0, D_2 = 0.52359$ $A_3 = 0.00016, B_3 = 0.00120, C_3 = 0, D_3 = 0.0150$	

The position, velocity and acceleration graphs in the joint space created for each actuator are given in Figure 6.9.

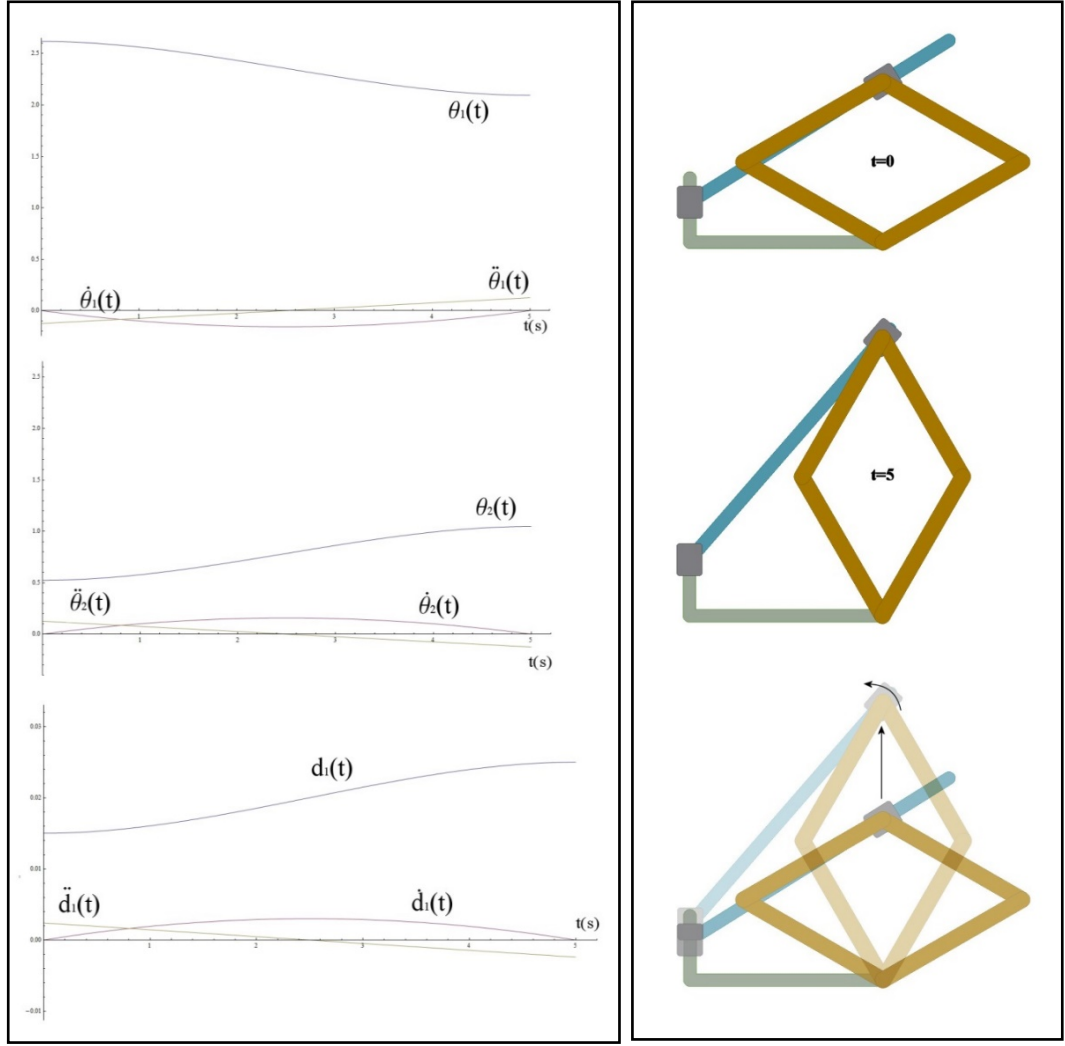


Figure 6.9: Actuator position velocity and acceleration graphs

The relevant trajectories were used in two different scenarios, modeled by adjusting the endpoint orientation of the macro manipulator so that the gravity direction is perpendicular to the micro manipulator plane  ${}^G\mathbf{R}_1$  and  ${}^G\mathbf{R}_2$  parallel (Equation 6.25).

$${}^G\mathbf{R}_1 = \begin{bmatrix} 1 & 0 & 0 \\ 0 & 1 & 0 \\ r_{31} = 0 & r_{32} = 0 & 1 \end{bmatrix}, \quad {}^G\mathbf{R}_2 = \begin{bmatrix} \cos \frac{\pi}{2} & 0 & \sin \frac{\pi}{2} \\ 0 & 1 & 0 \\ r_{31} = -\sin \frac{\pi}{2} & r_{32} = 0 & \cos \frac{\pi}{2} \end{bmatrix} \quad (6.25)$$

The results obtained from the theoretical and simulation environment were compared and it was seen that the results were consistent with each other (Figure 6.10-6.11).

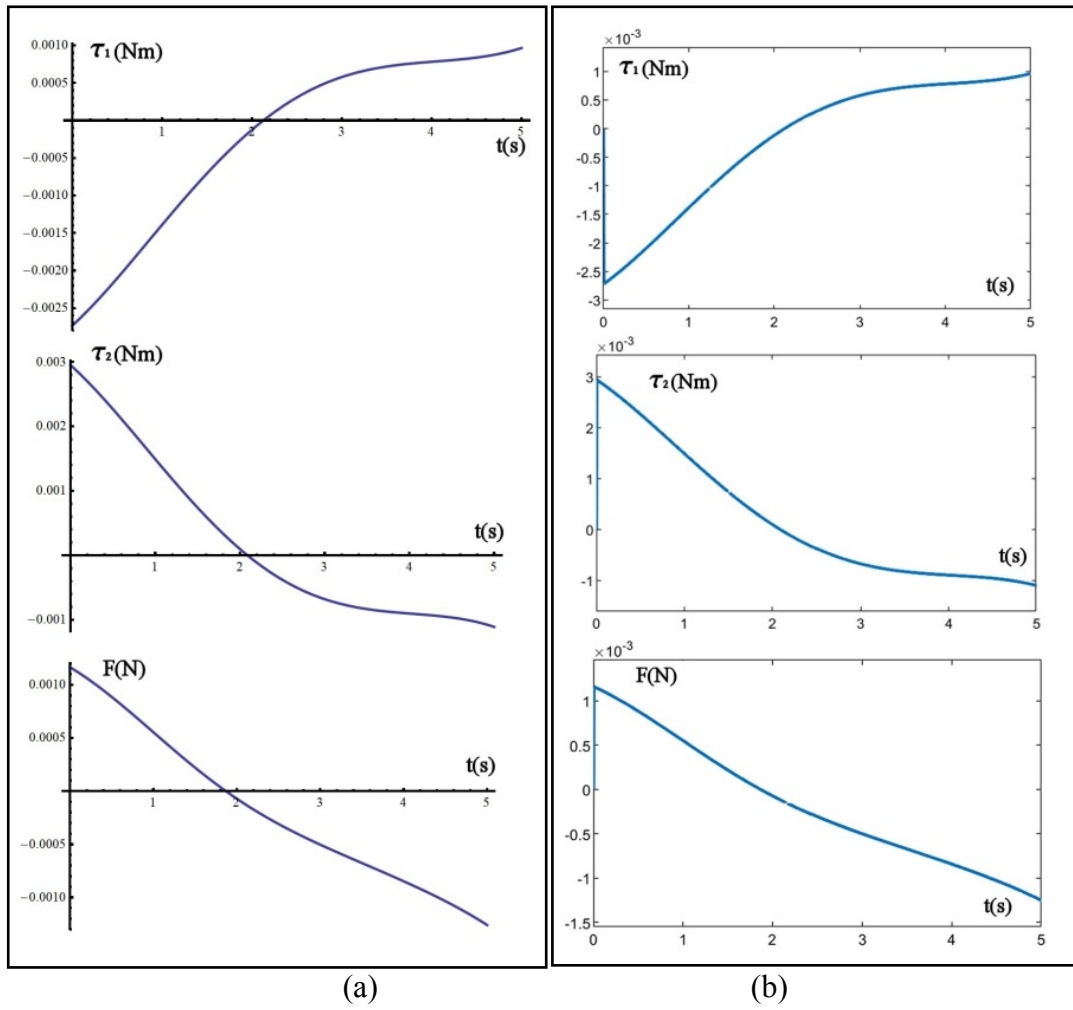


Figure 6.10: Result comparison a) Theoretical actuator torques and forces ( ${}^{\mathcal{C}}\mathbf{R}_1$ ) (Mathematica), b) Simulation environment actuator torque and force ( ${}^{\mathcal{C}}\mathbf{R}_1$ ) (Matlab SimMechanics)

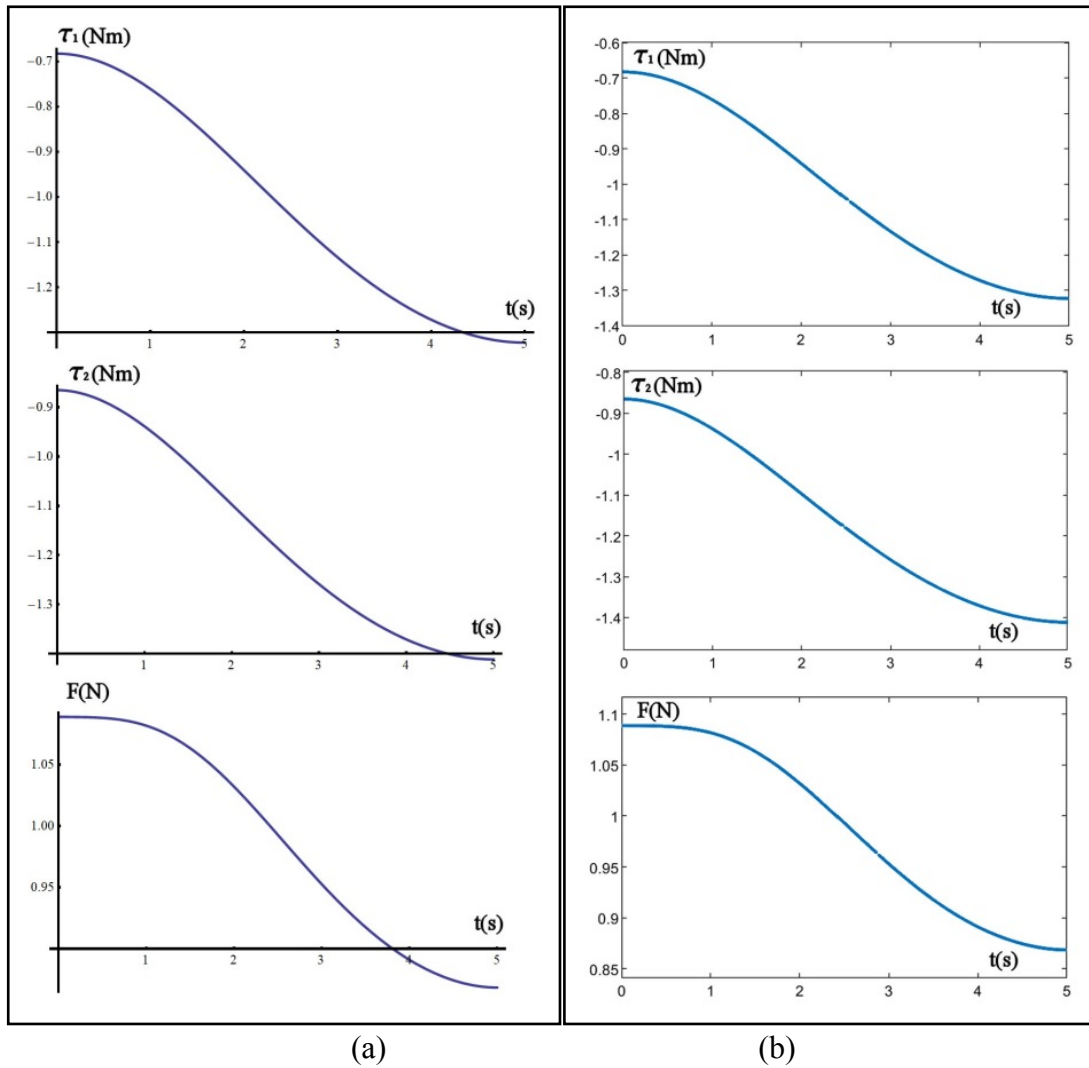


Figure 6.11 Result comparison a) Theoretical actuator torques and forces ( ${}^G\mathbf{R}_2$ ) (Mathematica), b) Simulation environment actuator torque and force ( ${}^G\mathbf{R}_2$ ) (Matlab SimMechanics)

The dimensions of the micro manipulator links used in the validation study process were determined to reach an efficient working volume. In addition, in order to determine actuator torque requirements according to the worst-case scenario, electromagnet masses were accepted as 1 kg and the remaining micro-manipulator link masses were determined to reach 80% of the macro manipulator load limit. It should be stated here that the values given in Table 6.2 covers only one side of the micromanipulator.

Tablo 6.2: Micro manipulator physical sizes determined for verification

<b>Mass (kg)</b>	<b>Mass Moment of Inertia (kg m<sup>2</sup>)</b>
$m_1 = m_2 = m_3 = m_4 = 0.250$ $m_5 = 1$ $m_6 = 0.136$ $m_7 = 0.364$	$I_{ww1} = I_{ww2} = I_{ww3} = I_{ww4} = 0.000244703$ $I_{ww5} = 0.000057258$ $I_{ww6} = 0.000008227$ $I_{ww7} = 0.001170830$
<b>Link Lengths (m)</b>	
$l = 0.1, d_2 = 0.12, d_3 = 0.19$	

# Chapter 7

## Constructional Design and Prototyping

Following the theoretical studies, the three-dimensional CAD model of the micro manipulator, whose kinematic structure of one half is shown in Figure 6.1, was constructed ready for prototype production of each assembly part (Figure 7.2).

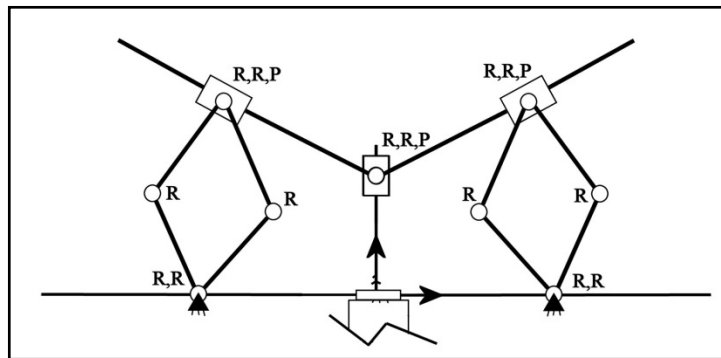


Figure 7.1: Micro manipulator kinematic structure

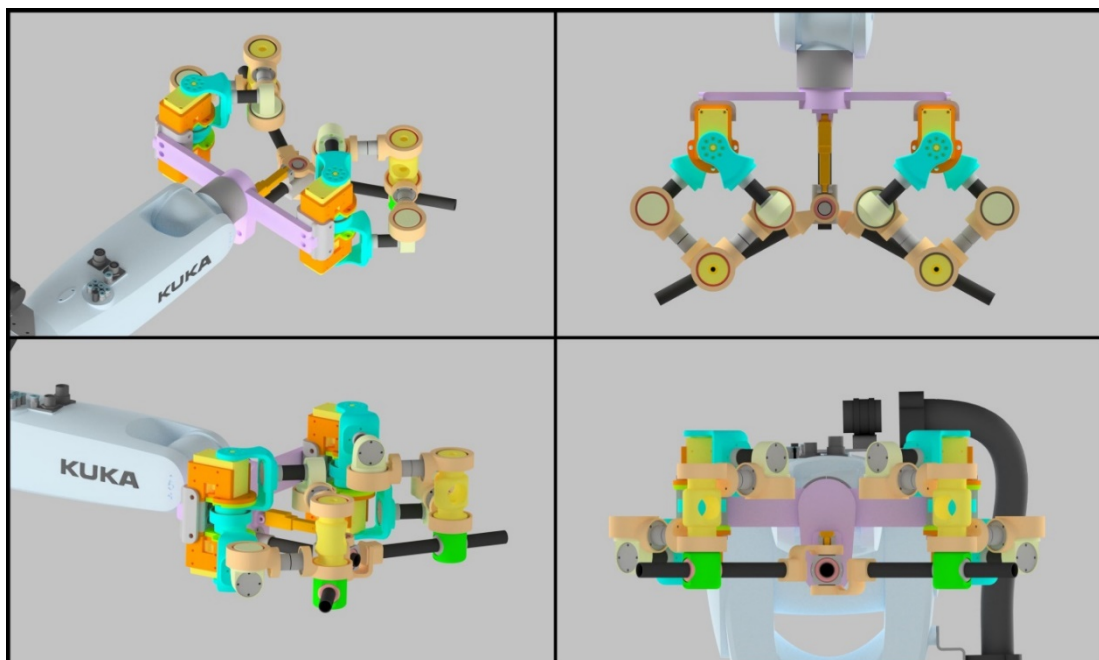


Figure 7.2: Micro manipulator conceptual design

The micromanipulator, whose three-dimensional structural model is seen in Figure 7.2, has a single linear actuator of the kinematic structure shown in Figure 6.1, in order to realize the translation ( $d_2$ ) movement of the electromagnet pairs of which  $d_1$  and  $\theta_1$  parameters have been determined. It was obtained by combining it in pairs (Figure 7.1). Although the rotation ( $\theta_1$ ) on their own axes and the translation ( $d_1$ ) movements on the axis between the electromagnets are also considered symmetric in the relevant motion scenario, the five-rod mechanisms on both sides of the micro manipulator are left active in order to give freedom to the ongoing thesis process. The micro manipulator created in this way can activate two electromagnets with five independent degrees of freedom. At this point, it should be noted that the actuators of the five bar mechanisms are operated synchronously and all the desired symmetrical movements can be realized.

In the process of the actuator selection of the relevant micromanipulator structure, although the macro manipulator orientation will never be adjusted to be parallel to the plane of the micromanipulator in the operation process, as in the scenario realized in the simulation environment, this situation has been accepted as the worst-case scenario, as shown in Figure 6.11. Considering the data obtained and the external forces that the electromagnet pairs will create at the time of working on each other, it has been decided to use the micro manipulator actuators as "Dynamixel XM540-W270-R" smart servo and "Actuonix L12-I" micro linear actuator (Figure 7.3). Some technical features of the selected actuators are specified in Table 7.1.



Figure 7.3: Micro manipulator actuators



Table 7.1: Technical specifications of micro manipulator actuators

<b>Technical Specifications</b>	<b>Dynamixel XM540-W270-R</b>	<b>Actuonix L12-I</b>
Max Torque/Force	12.9 Nm	22 N
Operating voltage	11.1 - 14.8 V	6 V
Current (Stall)	5.5 A @14.8 V	0.46 A
Transmission Rate	272.5:1	50:1
Mass	165 g	34

## 7.1 Micromanipulator Prototype Production

The conceptual design and all analysis processes (kinematic and dynamic) of the updated micromanipulator structure were completed and the prototype production phase was started using three-dimensional part designs ready for assembly and production (Figure 7.4).

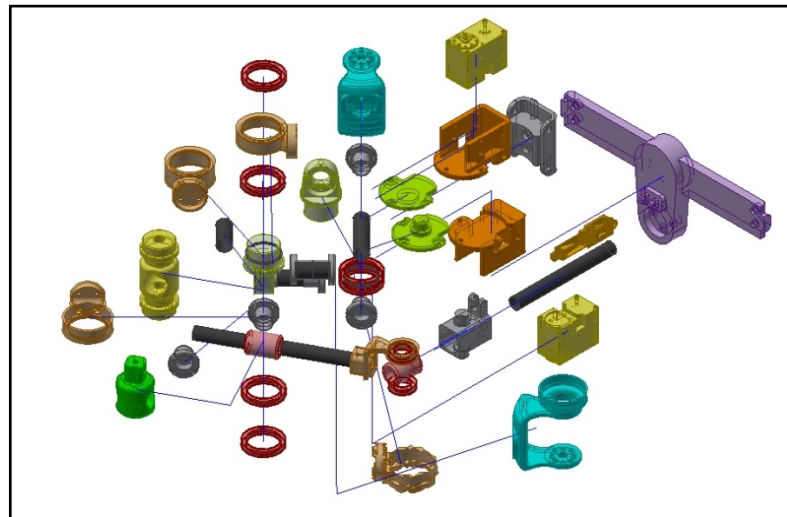


Figure 7.4: Micromanipulator part designs (Other symmetrical half of system not shown)

The first prototype production studies of the manipulator were started using the Zortrax M200 rapid prototyping system and ABS material, like the other prototype productions realized within the scope of the project. However, the geometric

complexity of the parts created inconsistencies on the printing surface due to the lifting off the table (Figure 7.5).



Figure 7.5: Initial prototype production trials Zortrax M200

At this point, it was decided to continue the prototype production by using the ABS-Plus filament material within the structure of the Stratasys Uprint SE rapid prototyping system, which is an industrially more professional three-dimensional printer.

In this way, the possibility of parts getting off the table during the printing process is prevented in the system, which has a printing volume that is closed and protected from external effects. In addition, thanks to the system's use of double nozzles, the part supports are made of fusible material, and the tolerance efficiency on the part after production is increased. The production and assembly stages of the parts with the rapid prototyping system is shown in Figure 7.6-7.9.

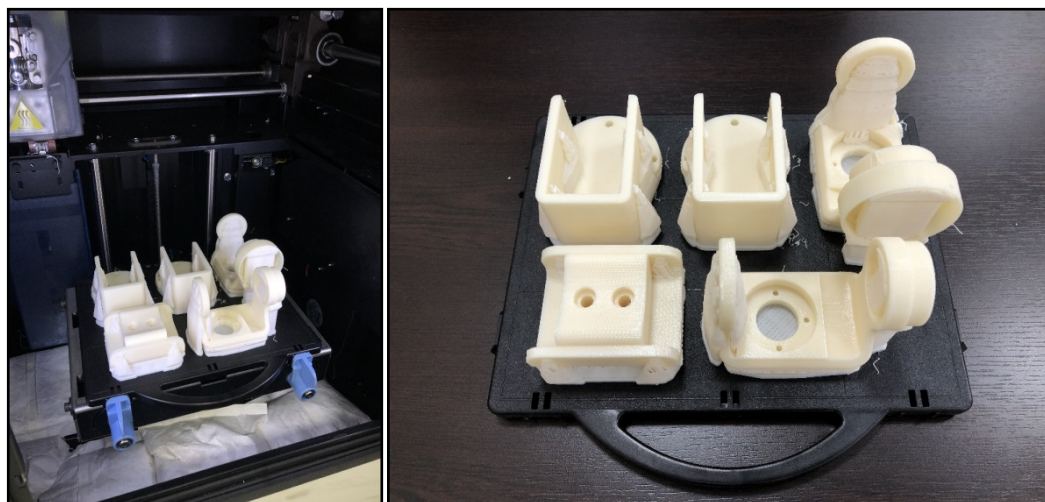


Figure 7.6: Prototype production stages

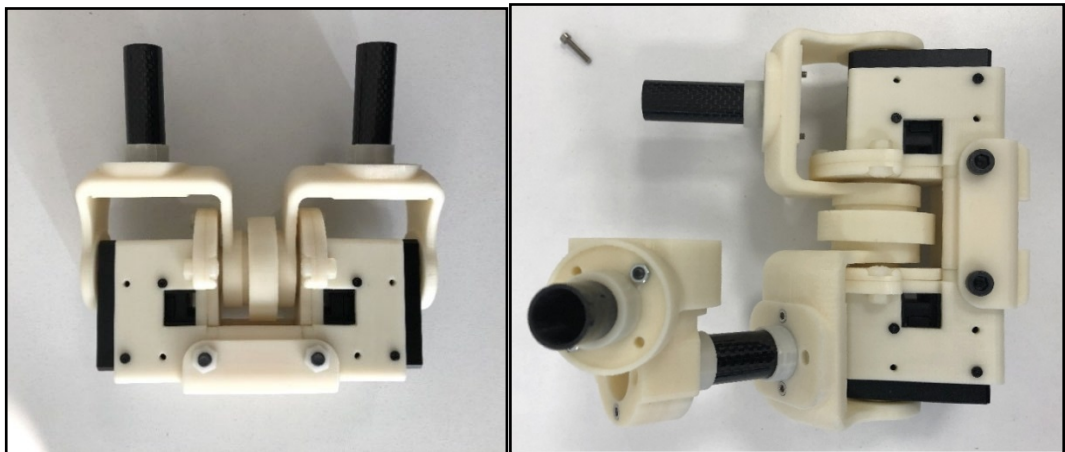
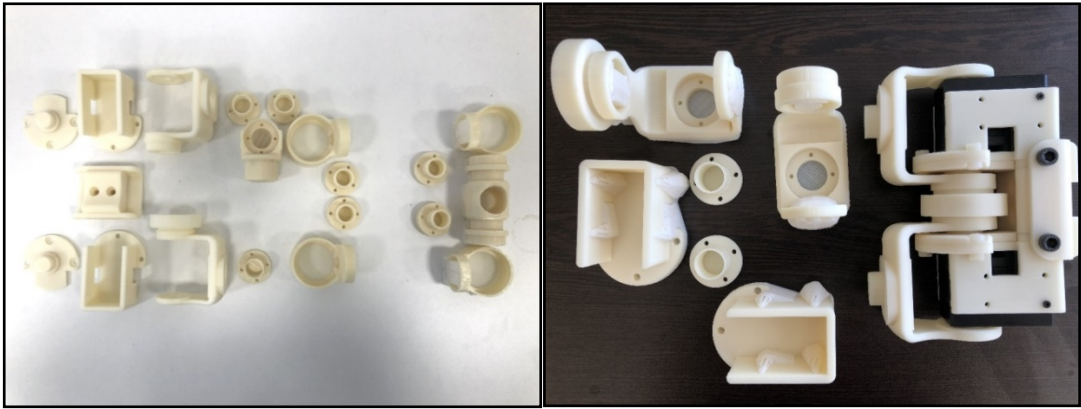


Figure 7.7: Prototype production and assembly stages (Actuator and carbon limbs assembly)

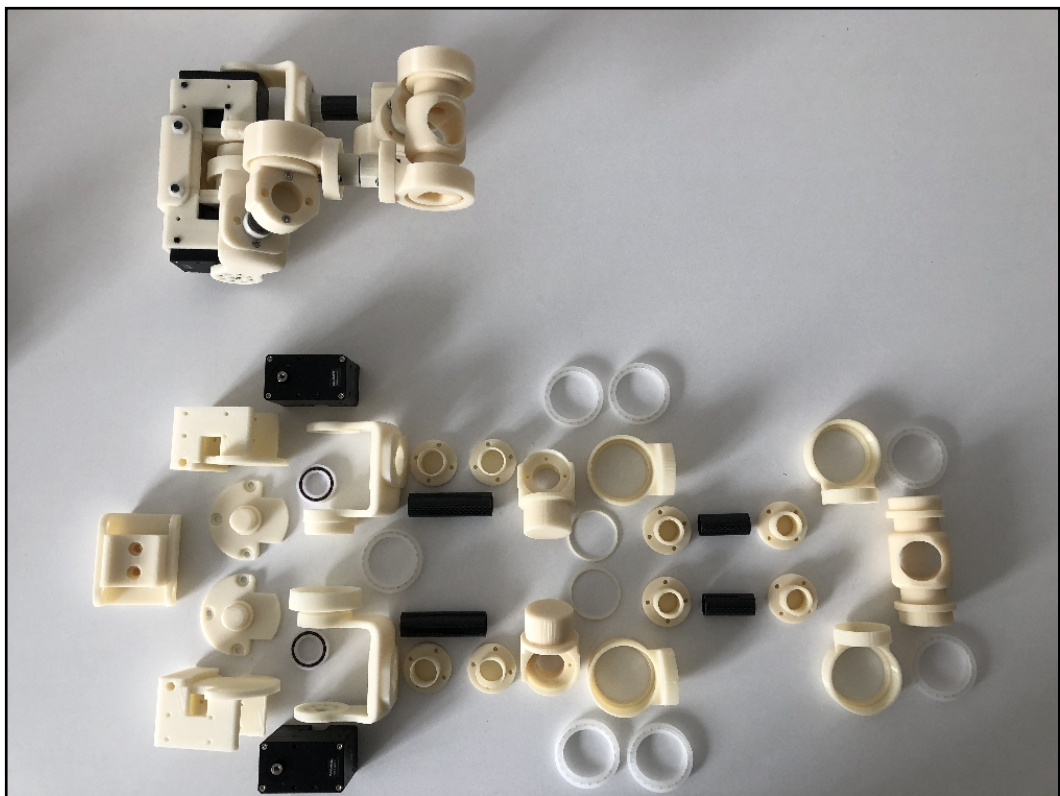


Figure 7.8: Micro manipulator assembly steps

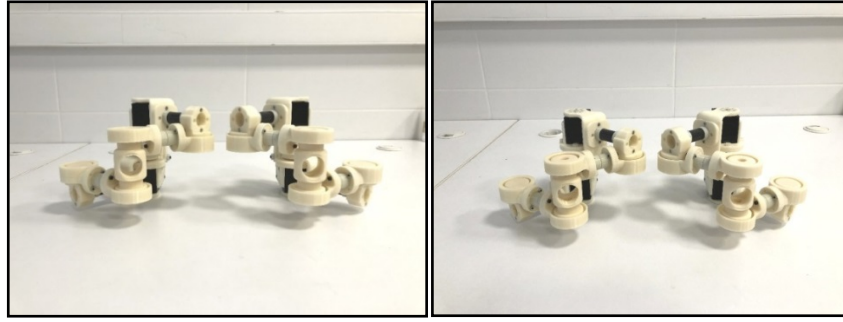


Figure 7.9: Split micro manipulator arms assembled & completed

Following the assembly process of the micro manipulator symmetrical arms, the production of the body that will form the base of the system where the arms will be connected and the connection with the macro manipulator has been started. As a material plexi glass material chosen for ease the cutting operations, if the material specifications are not fulfills the stability of the system supplementary parts are introduced. Since the relevant part will remove all the load related to the micro manipulator, it has been decided to produce the production using conventional production techniques in the Güngör Makina GM MILL CNC three-axis machining center, located in our laboratory, instead of rapid prototyping. Production of the surgical navigation mock-up part, the coding and simulation phase required for the production of the floor part, whose design and dimensioning was completed, in CNC was carried out in the Siemens SinuTrain simulation program, which is fully compatible with the Siemens Sinumerik 828D controller on the system. After the codes written in the Siemens SinuTrain simulation program were transferred to the Siemens Sinumerik 828D controller, the piece to be processed was connected to the CNC table, the reset process was performed and the production phase was started (Figures 7.10 – 7.11). CNC parameters used in the production phase are given in Table 7.2.

Table 7.2: CNC production parameters

Parameter	Specification
Cutting Tool	M4 Shank Milling Cutter
Chuck Speed	2000 rev/min
Feeding Speed	0.5 mm/thread
Tolerance	0.01 mm

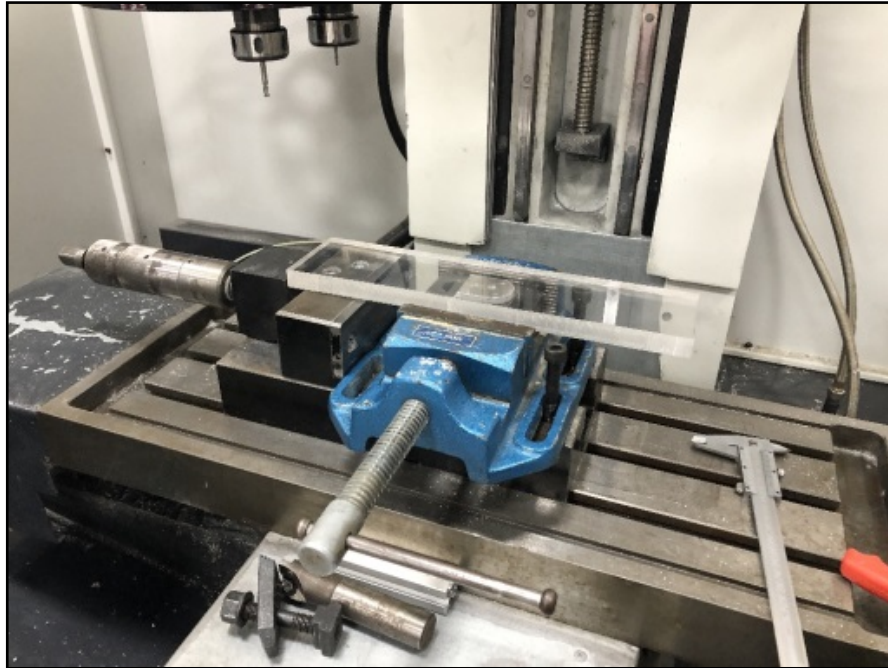


Figure 7.10: Connecting the plexi glass part to the CNC table

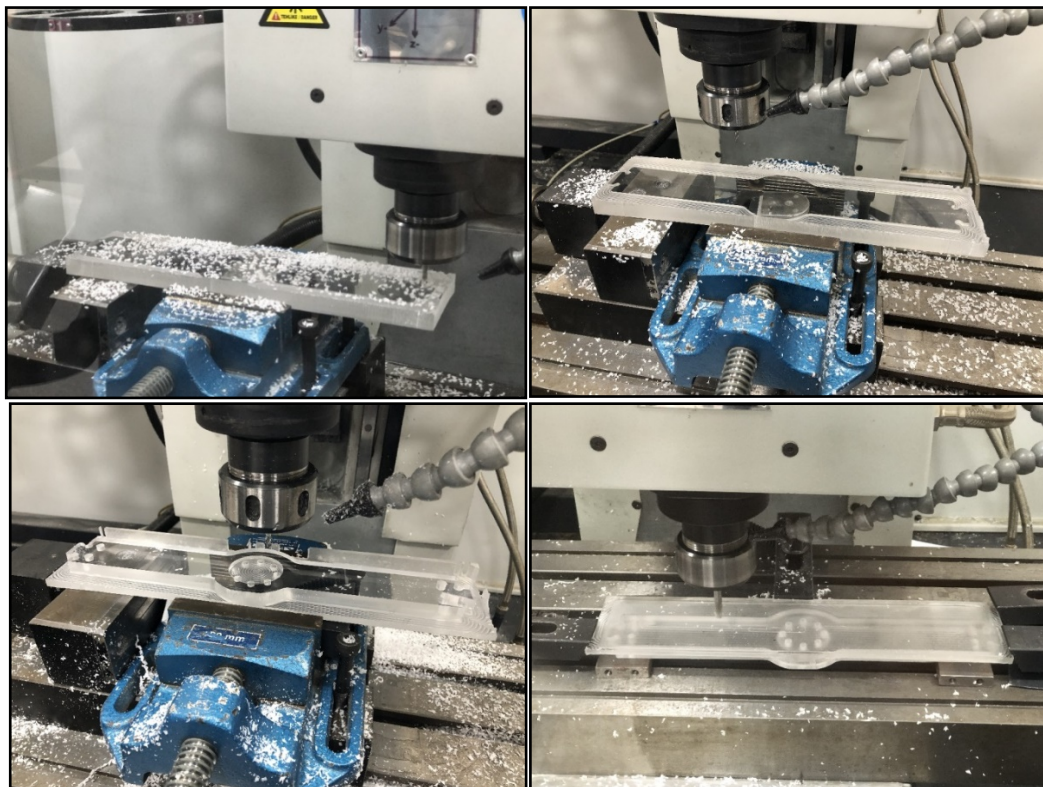


Figure 7.11: Production of Micro Manipulator Floor

In order for the micro manipulator, to work independently of the macro manipulator, a main base was created from aluminum sigma profiles and the whole system was successfully assembled on the relevant base with the production of the missing parts by rapid prototyping (Figures 7.12 – 7.13).

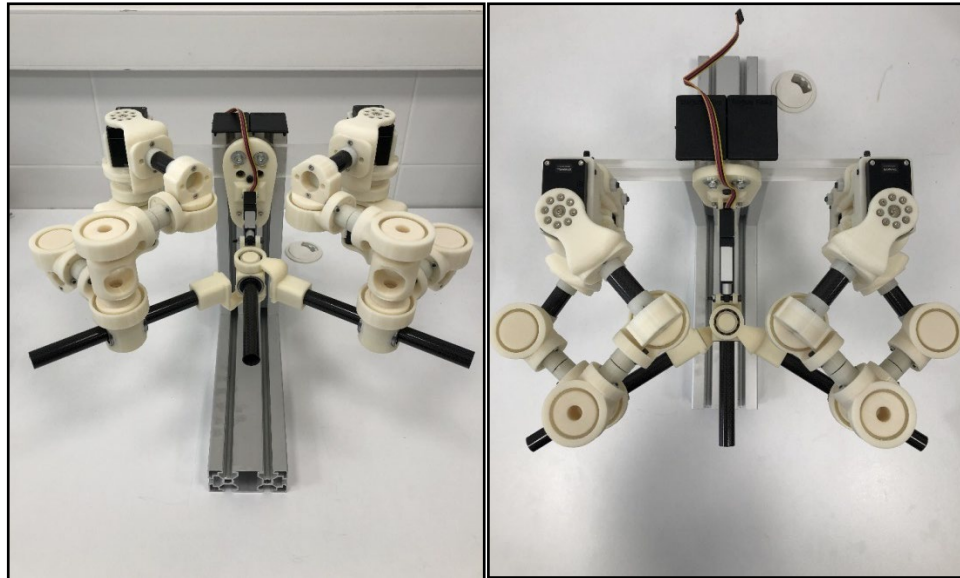


Figure 7.12: Completed micro manipulator assembly I

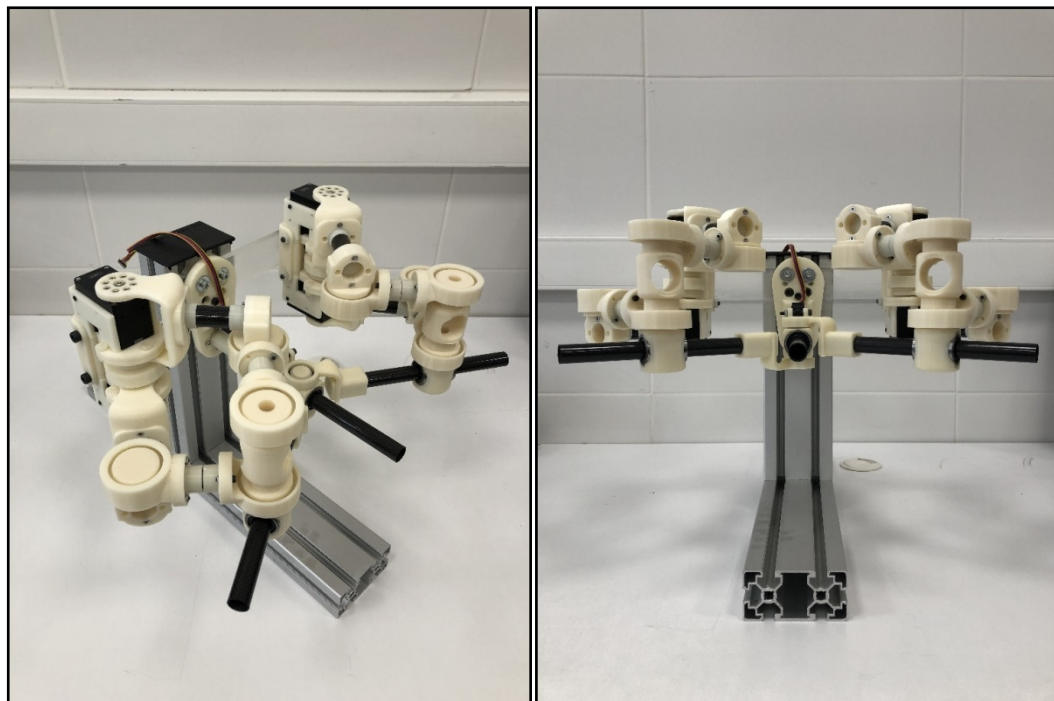


Figure 7.13: Completed micro manipulator assembly II

As can be seen in Figures 7.12 and 7.13, care has been taken to use polymer fasteners (bolts, bearings, etc.) on the system assembly as much as possible..

## 7.2 Supplementary Studies

In order to prevent bendings on the system while having the more precise movements of actuators, additional features added to the system. As a first for the "Dynamixel XM540-W270-R" actuators, when activators are in operational mode, bending

observed on the Plexi Glass base structure. Thus, new part designed and manufactured with rapid prototyping.

Before the motion verification studies of the completed prototype production of micro manipulator, it's important to have precise movements on the manipulator, in other words more robust system design.

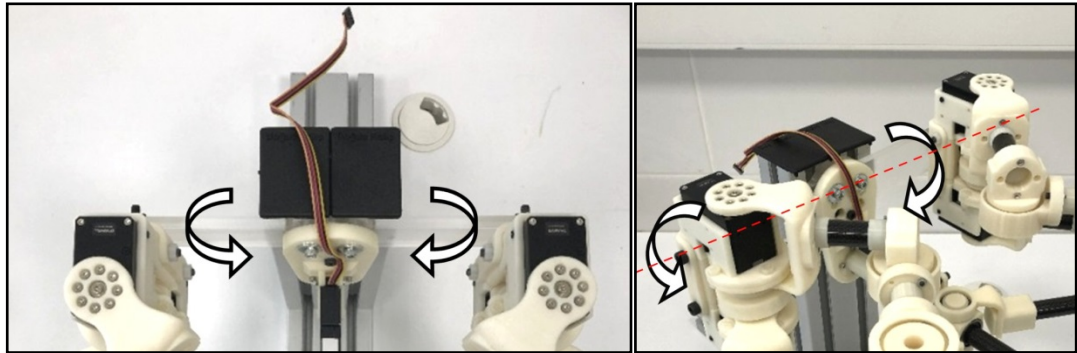


Figure 7.14: Possible deformations that may occur on the micro manipulator ground  
In order to prevent possible deformations (Figure 7.14) that may occur on the manipulator ground during the measurement and verification studies, parts that will form a federate structure between the manipulator ground and the aluminum base consisting of sigma profiles to be used in the preliminary test studies were designed and prepared. Assemblies were made on the system (Figure 7.15).

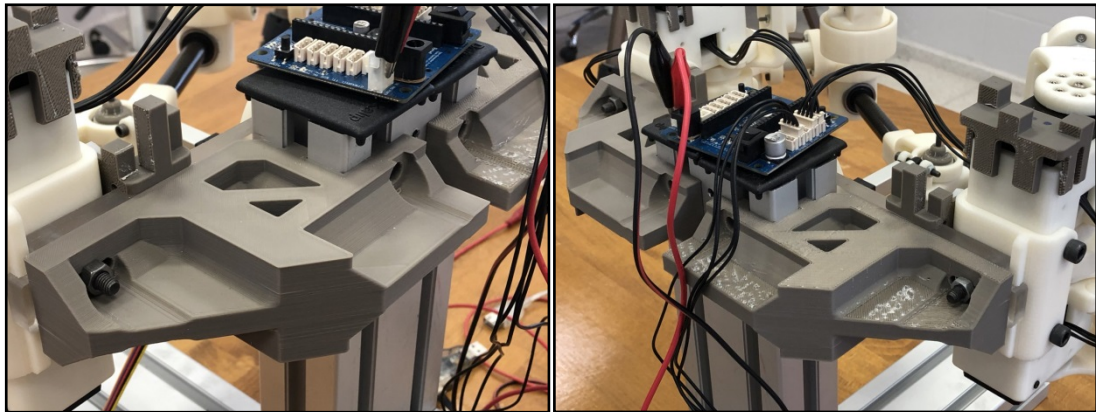


Figure 7.15: Support parts designed between micro manipulator base and aluminum

# Chapter 8

## Hardware Verification

Within the scope of surgical navigation studies, the physical measurement space in which motion capture cameras are located and the virtual reality space in which virtual models are visualized are associated with each other (Figure 8.1). By using the methodology created and followed in this direction in a similar way, the micro manipulator can also be integrated into motion verification studies.

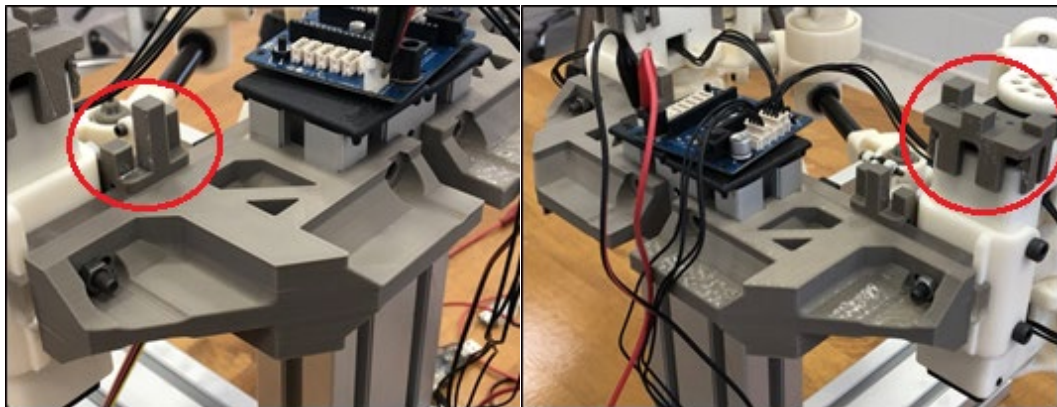


Figure 8.1: Parts designed for relation of physical measurement space and virtual reality space

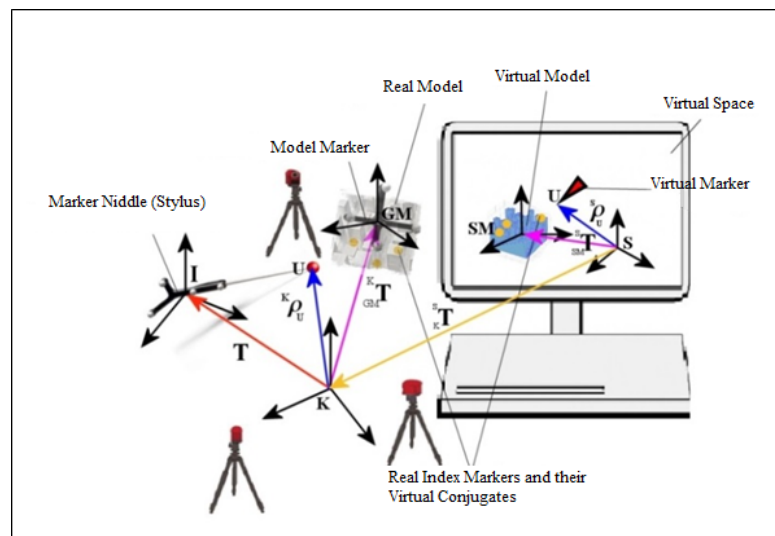


Figure 8.2: Relation of physical measurement space and virtual reality space



However, in order for the motion verification studies to be carried out with the help of cameras, the  ${}^{K}_{MM}\mathbf{T}$  and  ${}^{S}_{MM}\mathbf{T}$  transformation strings of the micro manipulator reference system to be placed in the physical measurement space must be calculated and associated with the camera measurement and virtual reality space (Figure 8.3).

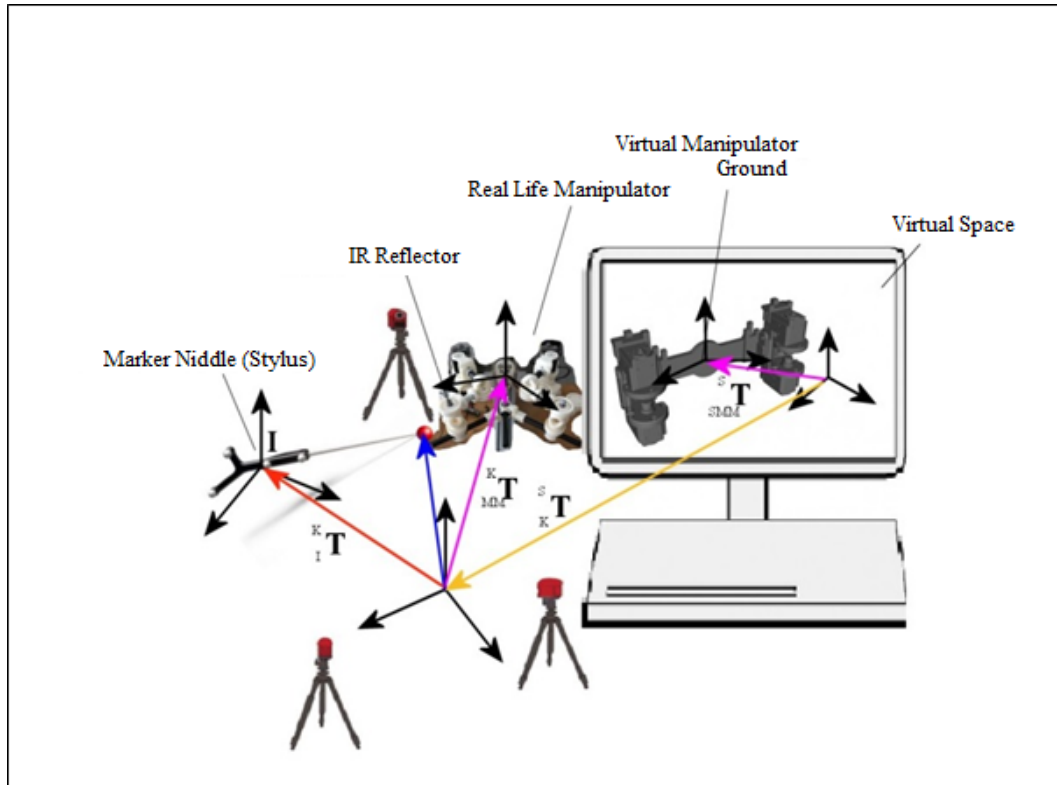


Figure 8.3: Relation of micro manipulator reference with physical measurement space and virtual reality space

At this point, in order to be able to take the necessary measurements, a mockup model produced within the scope of the thesis, like the mockup model, on the micro manipulator, the locations of which are known precisely according to the manipulator reference, were needed. In this regard, determining zone apparatuses that can be mounted on the system were designed, produced by rapid prototyping method and mounted on a micro manipulator (Figure 8.4).



Figure 8.4: Decisive zone apparatus mounted on micro manipulator

In this way, using the marker needle designed in the first reporting period, measurements will be taken from the index points on the relevant parts during the matching process.

The  ${}^K_T$  transform string containing the position and orientation information of the marker needle in the measurement space is created by the motion capture software, and the  ${}^{SMM}_T$  transform string containing the position and orientation information in the virtual reality space of the micro manipulator model created by adding the determinant region apparatuses is created by the 3D Slicer software.

In addition, the position of the tip point of the marker needle in the measurement space ( ${}^K_{\rho_U}$ ) is known thanks to the fixed geometry of the marker and the marker needle pivot calibration, the process of which was detailed in the first reporting period.

In this regard, 100 measurements were taken (Figure 8.5) from each of the index marks on the determinant zone apparatus by using the marker needle point to minimize the uncertainty of the tracking system, and the average of 100 measurements was used for the relevant location to be used in the calculation.

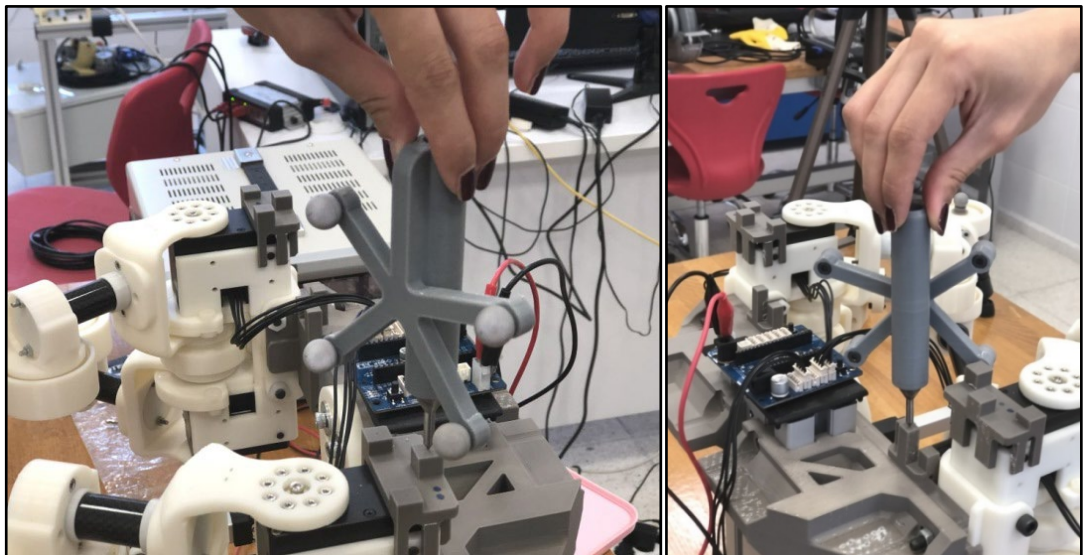


Figure 8.5: Taking measurements on decisive zone apparatus

The equivalents ( ${}^S_{\rho_U}$ ) of the obtained positions in the virtual reality space were marked in the 3D Slicer software with the help of the virtual marker (mouse cursor) and determined by the software (Figure 8.5).

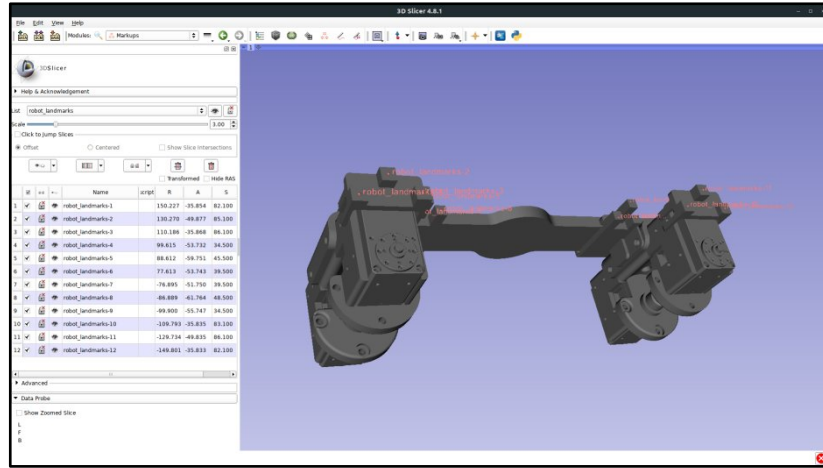


Figure 8.6: Identification of virtual reality environment index markings

By using the known three-dimensional point sets ( ${}^K \mathbf{p}_U$ ,  ${}^S \mathbf{p}_U$ ), ( ${}^S \mathbf{p}_U$ ,  ${}^{MM} \mathbf{p}_U$ ), and ( ${}^K \mathbf{p}_U$ ,  ${}^{MM} \mathbf{p}_U$ ) obtained during this process in the least squares method, the details of which were presented in the first reporting period,  ${}^S \mathbf{T}_K$ ,  ${}^{SMM} \mathbf{T}$  and  ${}^{KM} \mathbf{T}$  transformation strings giving the least square mean error are obtained.

In addition, at this stage, parts to which passive IR reflectors can be connected to micro-manipulator endpoint positions were designed (Figure 8.7) and produced. In this way, the manipulator endpoints will be followed by cameras during a movement to be performed in verification studies.

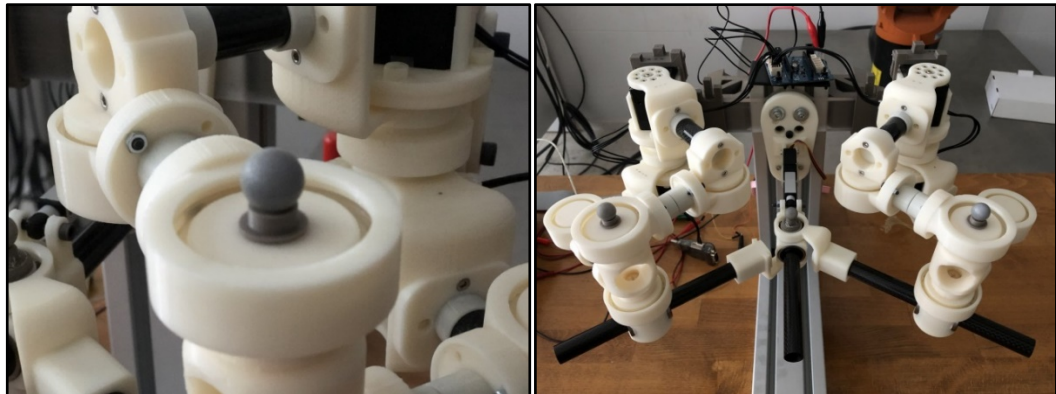


Figure 8.7: Micro manipulator endpoint passive IR reflector connectors

As a result of the studies, the measurement space and the micro manipulator reference system were associated with each other with an error of 0.376 mm RMS. In order to carry out the verification studies of the micro robot manipulator, the trajectories to be followed by the manipulator endpoints were determined and the targeted actuator trajectories were reached by passing from the task space to the joint

space by using the micro manipulator kinematic analysis equations used from before sections (Figure 8.8).

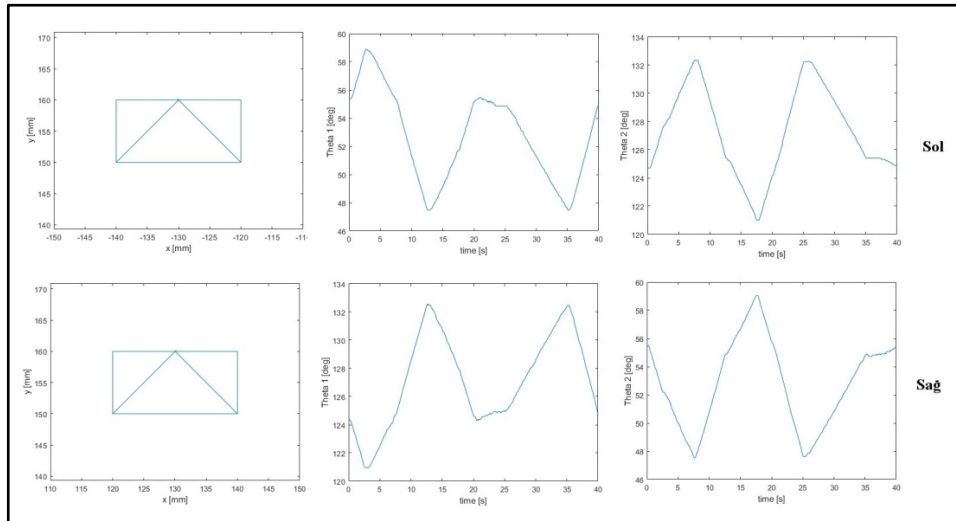


Figure 8.8: Manipulator endpoint traces and actuator trajectories dedicated to follow Within the scope of validation studies, Dynamixel SDK 3.4.2 and Dynamixel Matlab Simulink libraries specially created by the manufacturer for Dynamixel actuators were used in order to send the desired motion commands to the actuators. In this context, the connection between the computer and the actuators is realized with the USB2Dynamixel hardware, while the power requirement of the actuators is met via the Dynamixel Open CM 485 card. At this point, each of the manipulator actuators is given a different identification number, and the four actuators are connected to each other in a serial daisy chain (Figure 8.9). The software in the Matlab Simulink environment created for sending motion commands is also visualized in Figure 8.10.

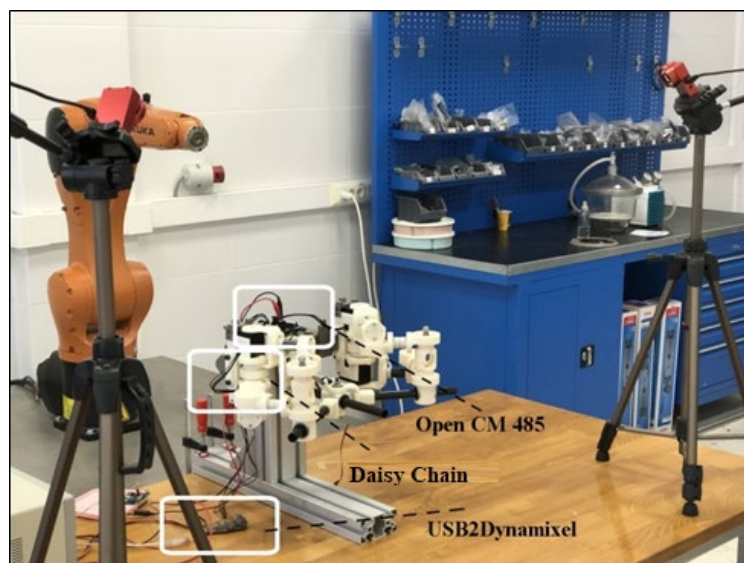


Figure 8.9: Hardware installation

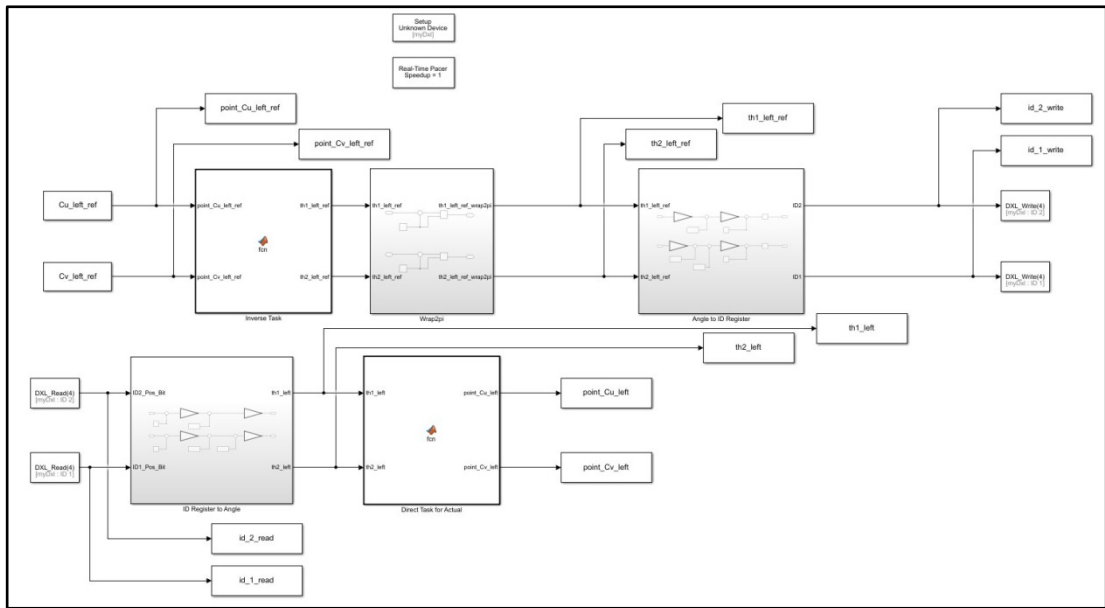


Figure 8.10: Sending motion commands to actuators via Matlab Simulink

The trajectory followed by both endpoints during the validation study was monitored by motion capture cameras and the measurement results were compared with the targeted endpoint traces (Figure 8.11).

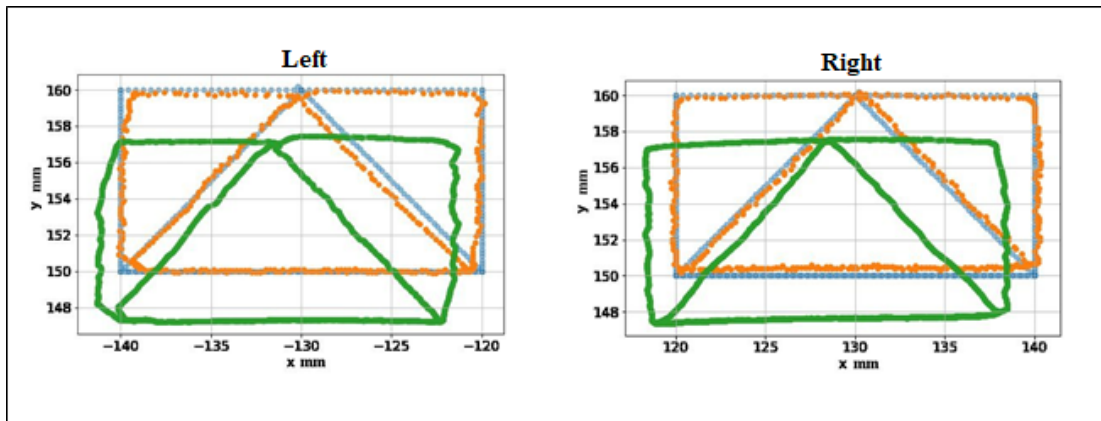


Figure 8.11: Validation Studies (Initial Measurement)

The graph indicated in blue are the traces that the micromanipulator endpoints (Right and Left) want to follow. The endpoint traces obtained by inserting the data from the actuator encoders into the further analysis equations are shown in orange. Both graphs confirm that the actuators successfully follow the desired motion in the joint space.

However, the trace, which is shown with green color, which is drawn by transferring the measurement data taken from motion capture cameras to the micro manipulator reference system, and which is actually followed by the manipulator endpoint, is

homogeneously offset in both the x-axis (1.45 mm) and the y-axis (2.4 mm). This indicates that there are fixed link size uncertainties on the system due to rapid prototyping production and assembly process.

Since the relevant deviations have a homogeneous structure, the deviation amounts were included in the trajectory calculation process and the compensation approach was adapted to the system and the actuator trajectories were recalculated for the same endpoint motion (Figure 8.12).

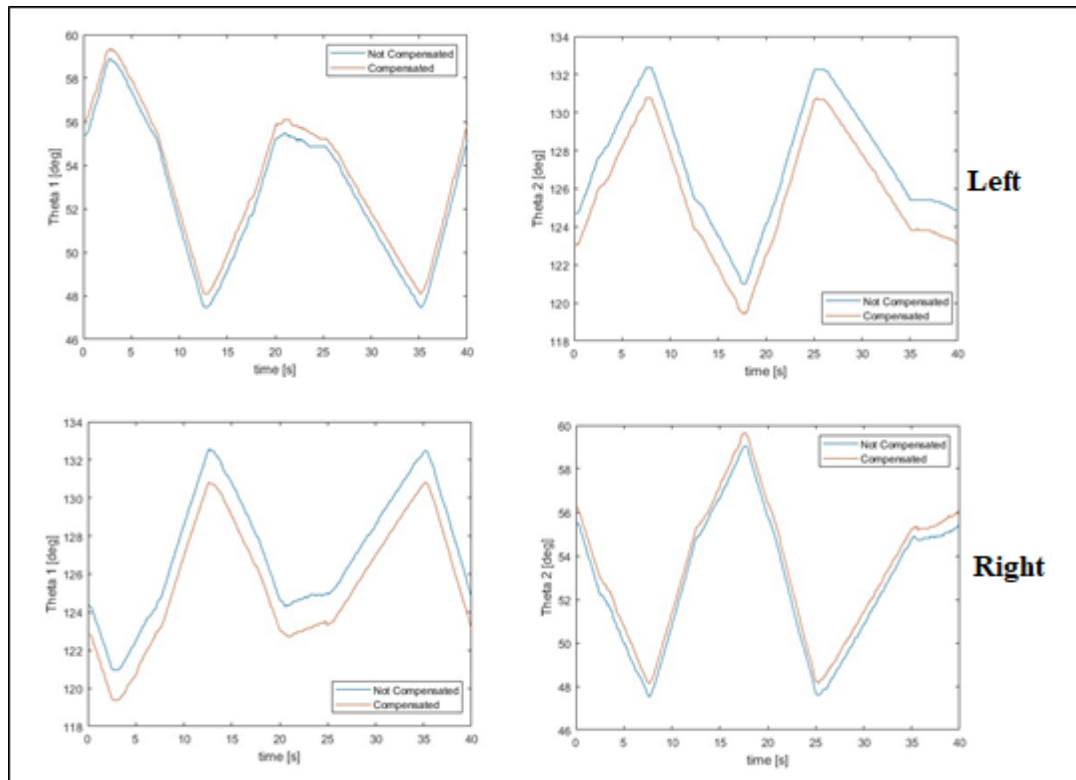


Figure 8.12: Compensated joint space actuator trajectories

As a result of repeated movement, it was seen that all three graphs overlapped as desired and the compensation was successful (Figure 8.13). At this point, the root means square error (RMS) between the camera measurement space and the micromanipulator reference system should be taken into account in order to evaluate the graphics correctly.

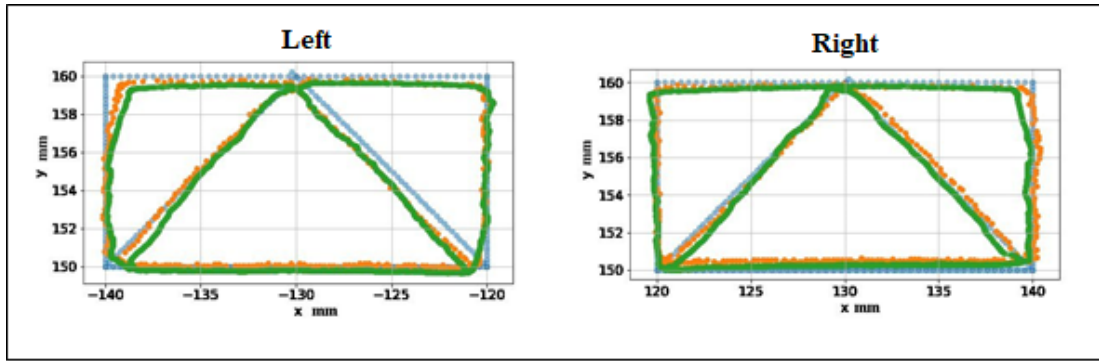


Figure 8.13: Confirmation studies (Compensation) In addition, in order to prove that the relevant compensation coefficients are consistent in different trajectories, the micromanipulator endpoints were allowed to follow a second trajectory and the obtained data were compared (Figure 8.14).

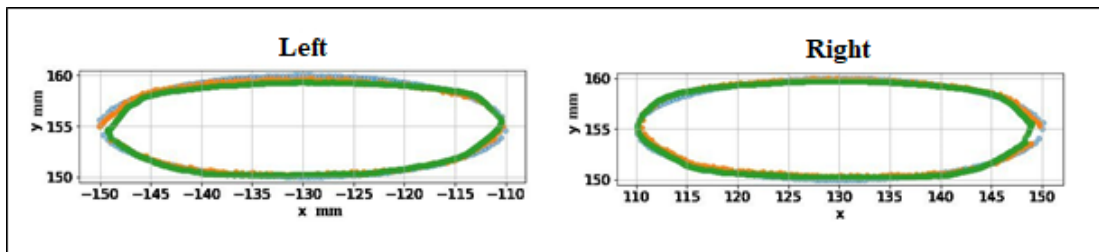


Figure 8.14: Validation Studies (New trajectory)

As can be seen in Figure 8.14, it was seen that the graphs overlapped as a result of the study. Thus, the designed micromanipulator verification studies were carried out successfully. Work on hardware will continue to increase tracking sensitivity.

# Chapter 9

## Conclusion

Throughout the thesis conceptual design of a macro-micro robot manipulator that will be utilized in untethered cochlear microrobot operations was proposed. Prior to the structural design workspace constraints of the micro manipulator and the location of cochlea was determined by using antropometric data of adult humans. Using acquired results early structure of the micro manipulator was introduced along with kinematic synthesis procedures during link length calculations. Due to the payload limits of the macro manipulator, although optimization procedure was carried out, achieved constructional parameters proved to be inadequate for the given constraints. From this point motional constraints of the manipulation scenerio were updated.

In light of this, structural design of a new 5 DoF parallel manipulator that will be utilized as a micro manipulator portion of a macro-micro medical robot was successfully proposed for microrobot stem cell homing procedures. Considering design constraints kinematic structure of the manipulator was introduced. Both theoretical kinematic and dynamic analysis procedures were described in detail. In order to verify theoretical approaches, simple model of the proposed manipulator was formed in Matlab SimMechanics simulation environment. It was shown that both of the theoretical and simulation results were consistent with each other. Prototype of the proposed manipulator successfully manufactured via rapid prototyping and the parts were assembled by utilizing nonmagnetic elements as much as possible. In order to verify path tracking performance of the manipulator, motion capture camera setup was prepared and relations between manipulator and camera workspaces were acquired by using surgical navigation registration techniques. During hardware verification steps, it was seen that manufactured manipulator has some dimensional uncertainties that causes homogeneous shift on its desired path



during the operation. In order to overcome this compensation amounts were calculated and compensated trajectories were fed to the system. Final test results promisingly showed that manufactured manipulator manages to follow desired end effector paths within a camera calibration error.

# References

[1] Blumenkranz, J. S., Prisco, G.M., DiMaio, S.P., Dachs, G.W., Dostmohamed, H., Hasser, C.J., Guthart, G.S., United States Patent No US20090248038A1.

[2] Ghodoussi, M.S.B., Mangaser, A.G., Uecker, D.S.B., Wang Y.G., Wright, J.S.B., German Patent and Trade Mark Office Patent No DE60222727T2

[3] Naus, G.J.L., Meenink, H.C.M., Beelen, M.J., De Smet, M.J.D., United States Patent No US20190038369A1

[4] Wenderow, T., Bromander, T., Kennedy, J.J., Thompson, S.O., Taylor, J.L., United States Patent No US20100076309A1

[5] Kang, H., United States Patent No US20140188132A1

[6] Hares, L.D.R., United States Patent No US20160331482A1

[7] Dahroug, Bassem & Brahim, Tamadazte & Tavernier, Laurent & Weber, Stefan & Andreff, Nicolas. (2018). Review on Otological Robotic Systems: Toward Micro-Robot Assisted Cholesteatoma Surgery. IEEE Reviews in Biomedical Engineering. PP. 1-1. 10.1109/RBME.2018.2810605.

[8] W. P. Liu, M. Azizian, J. Sorger, R. H. Taylor, B. K. Reilly, K. Cleary, and D. Preciado, "Cadaveric feasibility study of da vinci si- assisted cochlear implant with augmented visual navigation for otologic surgery," JAMA Otolaryngology-Head & Neck Surgery, vol. 140, no. 3, pp. 208-214, 2014.

[9] Kenngott HG, Fischer L, Nickel F, Rom J, Rassweiler J, Müller-Stich BP. Status of robotic assistance--a less traumatic and more accurate minimally invasive surgery? Langenbecks Arch Surg. 2012 Mar;397(3):333-41. doi: 10.1007/s00423-011-0859-7. Epub 2011 Oct 29. PMID: 22038293.

- [10] Singh, Ajay & Sitti, Metin. (2015). Targeted Drug Delivery and Imaging Using Mobile Milli/Microrobots: A Promising Future Towards Theranostic Pharmaceutical Design. *Current pharmaceutical design*. 22. 10.2174/1381612822666151210124326.
- [11] Edd, J. & Payen, S. & Rubinsky, Boris & Stoller, M.L. & Sitti, Metin. (2003). Biomimetic propulsion for a swimming surgical micro-robot. *Proceedings of the IEEE/RSJ international conference on intelligent robots and systems, Las Vegas, 2003 (IROS 2003)*. 2583 - 2588 vol.3. 10.1109/IROS.2003.1249259.
- [12] Dahroug, Bassem & Brahim, Tamadazte & Tavernier, Laurent & Weber, Stefan & Andreff, Nicolas. (2018). Review on Otological Robotic Systems: Toward Micro-Robot Assisted Cholesteatoma Surgery. *IEEE Reviews in Biomedical Engineering*. PP. 1-1. 10.1109/RBME.2018.2810605.
- [13] Amokrane, W. & Belharet, Karim & Souissi, Mouna & Grayeli, A. & Ferreira, Antoine. (2018). Macro-micro manipulation platform for inner ear drug delivery. *Robotics and Autonomous Systems*. 107. 10.1016/j.robot.2018.05.002.
- [14] Grady MS, Howard MA 3rd, Molloy JA, Ritter RC, Quate EG, Gillies GT. Nonlinear magnetic stereotaxis: three-dimensional, in vivo remote magnetic manipulation of a small object in canine brain. *Med Phys*. 1990 May-Jun;17(3):405-15. doi: 10.1118/1.596520. PMID: 2200950.
- [15] Cheon B, Gezgin E, Ji DK, Tomikawa M, Hashizume M, Kim HJ, Hong J. A single port laparoscopic surgery robot with high force transmission and a large workspace. *Surg Endosc*. 2014 Sep;28(9):2719-29. doi: 10.1007/s00464-014-3534-6. Epub 2014 May 2. PMID: 24789128.
- [16] World health Organization Deafness and Hearing Loss. [(accessed on 24 May 2018)]; Available online: [www.who.int/en/news-room/fact-sheets/detail/deafness-and-hearing-loss](http://www.who.int/en/news-room/fact-sheets/detail/deafness-and-hearing-loss). [Ref list]
- [17] Stone JS, Cotanche DA. Hair cell regeneration in the avian auditory epithelium. *Int J Dev Biol*. 2007;51(6-7):633-47. doi: 10.1387/ijdb.072408js. PMID: 17891722.

- [18] W Turner, Christopher & A.J. Reiss, Lina & J Gantz, Bruce. (2007). Combined Acoustic and Electric Hearing: Preserving Residual Acoustic Hearing. *Hearing research*. 242. 164-71. 10.1016/j.heares.2007.11.008.
- [19] Beisel, Kirk & Hansen, Laura & Soukup, Garrett & Fritsch, Bernd. (2008). Regenerating cochlear hair cells: Quo vadis stem cell. *Cell and tissue research*. 333. 373-9. 10.1007/s00441-008-0639-z.
- [20] Min Yong Lee (2018) Potential of Gene and Cell Therapy for Inner Ear Hair Cells
- [21] T.J. Thomas (2018) Gene Delivery into the Inner Ear and Its Clinical Implications for Hearing and Balance
- [22] Stone JS, Cotanche DA (2007) Hair cell regeneration in the avian auditory epithelium. *Int J Dev Biol* 51:633–647
- [23] Luiz Gustavo Dufner-Almeida, Dayane Bernardino da Cruz, Regina Célia Mingroni Netto, Ana Carla Batissoco, Jeanne Oiticica, Rodrigo Salazar-Silva, Stem-cell therapy for hearing loss: are we there yet?, *Brazilian Journal of Otorhinolaryngology*, Volume 85, Issue 4, 2019, Pages 520-529, ISSN 1808-8694, 10.1016/j.bjorl.2019.04.006.
- [24] W Turner, Christopher & A.J. Reiss, Lina & J Gantz, Bruce. (2007). Combined Acoustic and Electric Hearing: Preserving Residual Acoustic Hearing. *Hearing research*. 242. 164-71. 10.1016/j.heares.2007.11.008.
- [25] Beisel, Kirk & Hansen, Laura & Soukup, Garrett & Fritsch, Bernd. (2008). Regenerating cochlear hair cells: Quo vadis stem cell. *Cell and tissue research*. 333. 373-9. 10.1007/s00441-008-0639-z.
- [26] Min Yong Lee (2018) Potential of Gene and Cell Therapy for Inner Ear Hair Cells
- [27] T.J. Thomas (2018) Gene Delivery into the Inner Ear and Its Clinical Implications for Hearing and Balance

- [28] Andre Sharon, Neville Hogan, David E. Hardt, The macro/micro manipulator: An improved architecture for robot control, *Robotics and Computer-Integrated Manufacturing*, Volume 10, Issue 3, 1993, Pages 209-222, ISSN 0736-5845.
- [29] Gordon, C. C., Churchill, T., Clauser, C. E., Bradtmiller, B., McConville, J. T., Tebbetts, I., & Walker, R. A. (1989). Anthropometric survey of US Army personnel: Summary statistics, interim report for 1988. ANTHROPOLOGY RESEARCH PROJECT INC YELLOW SPRINGS OH.
- [30] Alasli, A., Çetin, L., Akçura, N., Kahveci, A., Can, F. C., & Tamer, Ö. (2019). Electromagnet design for untethered actuation system mounted on robotic manipulator. *Sensors and Actuators A: Physical*, 285, 550-565.
- [31] Gupta, R., Bartling, S. H., Basu, S. K., Ross, W. R., Becker, H., Pfoh, A., ... & Curtin, H. D. (2004). Experimental flat-panel high-spatial-resolution volume CT of the temporal bone. *American journal of neuroradiology*, 25(8), 1417-1424.
- [32] Bartling, S., Jakab, K., Kikinis, R. (2018). The SPL Inner Ear Atlas. The Open Anatomy Project, Surgical Planning Laboratory, Department of Radiology, Brigham and Women's Hospital, Harvard Medical School.
- [33] Kikinis, R., Pieper, S.D., Vosburgh, K. (2014). 3D Slicer: a platform for subject-specific image analysis, visualization, and clinical support. *Intraoperative Imaging Image-Guided Therapy*, Ferenc A. Jolesz, Editor 3(19):277–289 ISBN: 978-1-4614-7656-6 (Print) 978-1-4614-7657-3 (Online)
- [34] Fedorov, A., Beichel, R., Kalpathy-Cramer, J., Finet, J., Fillion-Robin, J-C., Pujol S., Bauer, C., Jennings, D., Fennessy, F.M., Sonka, M., Buatti, J., Aylward, S.R., Miller, J.V., Pieper, S., Kikinis, R. (2012). 3D Slicer as an Image Computing Platform for the Quantitative Imaging Network. *Magn Reson Imaging*. 30(9):1323-41. PMID: 22770690. PMCID: PMC3466397.
- [35] Salih, W. H., Buytaert, J. A., Aerts, J. R., Vanderniepen, P., Dierick, M., & Dirckx, J. J. (2012). Open access high-resolution 3D morphology models of cat, gerbil, rabbit, rat and human ossicular chains. *Hearing research*, 284(1-2), 1-5.

[36] Freudenstein, F., & Alizade, R. (1975, September). On the degree of freedom of mechanisms with variable general constraint. In Proceedings Fourth World Congress on the Theory of Machines and Mechanisms (pp. 51-56).

[37] Tsai, L. W. (1999). Robot analysis: the mechanics of serial and parallel manipulators. John Wiley & Sons.

# Appendices

# Appendix B

## Publications from the Thesis

### **Conference Papers**

1. Yasar A. E., Uslu T., Gezgin E., Çetin L, On the Conceptual Design of a Macro Micro Robot Manipulator for Cochlear Microrobot Operations: A Case Study on Cochlea Localization, 34th Florida Conference on Recent Advances in Robotics FCRAR 2021

### **Projects**

1. Project Fellow in The Scientific and Technological Research Council of Turkey with Project No: 218E055.



# Curriculum Vitae

Name Surname : Alp Emre Yaşar

## Education:

2012–2018 İzmir Kâtip Çelebi University, Dept. of Mechanical Eng.

2018–2021 İzmir Kâtip Çelebi University, Dept. of Mechanical Eng.

## Work Experience:

2020 – Cont. BOSCH Thermotechnology – Mechanical Design Engineer

## Publications:

Yasar A. E., Uslu T., Gezgin E., Çetin L, On the Conceptual Design of a Macro Micro Robot Manipulator for Cochlear Microrobot Operations: A Case Study on Cochlea Localization, 34th Florida Conference on Recent Advances in Robotics FCRAR 2021

## Projects

Project Fellow in The Scientific and Technological Research Council of Turkey with Project No: 218E055.